

UNCLASSIFIED

AD NUMBER

ADB005227

LIMITATION CHANGES

TO:

Approved for public release; distribution is unlimited.

FROM:

Distribution authorized to U.S. Gov't. agencies only; Test and Evaluation; 22 APR 1975. Other requests shall be referred to Air Force Avionics Laboratory, AFAL/RWI, Wright-Patterson AFB, OH 45433.

AUTHORITY

afwal ltr, 4 dec 1975

THIS PAGE IS UNCLASSIFIED

THIS REPORT HAS BEEN DELIMITED
AND CLEARED FOR PUBLIC RELEASE
UNDER DOD DIRECTIVE 5200.20 AND
NO RESTRICTIONS ARE IMPOSED UPON
ITS USE AND DISCLOSURE.

DISTRIBUTION STATEMENT A

APPROVED FOR PUBLIC RELEASE;
DISTRIBUTION UNLIMITED.

AD B005227

AFAL-TR-75-77

ERIM No. 105900-16-F

Final Report

REAL-TIME OPTICAL DATA MODULATOR

FOR PERIOD OCTOBER 1973 — NOVEMBER 1974

MAY 1975



Distribution limited to United States Government agencies only (Test and Evaluation); 22 April 1975. Other requests for this document must be referred to the Air Force Avionics Laboratory, (AFAL/RWI), Wright-Patterson Air Force Base, Ohio 45433.

AIR FORCE AVIONICS LABORATORY
AIR FORCE SYSTEMS COMMAND
WRIGHT-PATTERSON AIR FORCE BASE, OHIO 45433

ENVIRONMENTAL
RESEARCH INSTITUTE OF MICHIGAN
FORMERLY WILLOW RUN LABORATORIES, THE UNIVERSITY OF MICHIGAN
BOX 618 • ANN ARBOR • MICHIGAN 48107

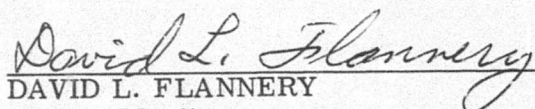
DDTC
RECEIVED
JUL 21 1975
RECEIVED

A

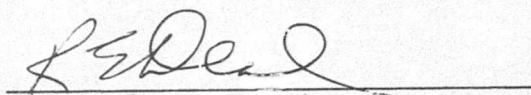
NOTICE

When Government drawings, specifications, or other data are used for any purpose other than in connection with a definitely related Government procurement operation, the United States Government thereby incurs no responsibility nor any obligation whatsoever; and the fact that the government may have formulated, furnished, or in any way supplied the said drawings, specifications, or other data, is not to be regarded by implication or otherwise as in any manner licensing the holder or any other person or corporation, or conveying any rights or permission to manufacture, use, or sell any patented invention that may in any way be related thereto.

This technical report has been reviewed and is approved for publication.


DAVID L. FLANNERY
Project Monitor

FOR THE DIRECTOR


ROBERT E. DEAL, Chief
Laser & E-O Technology Branch
Electronic Technology Division

Copies of this report should not be returned unless return is required by security considerations, contractual obligations, or notice on a specific document.

UNCLASSIFIED

SECURITY CLASSIFICATION OF THIS PAGE (When Data Entered)

REPORT DOCUMENTATION PAGE		READ INSTRUCTIONS BEFORE COMPLETING FORM
1. REPORT NUMBER AFAL-TR-75-77	2. GOVT ACCESSION NO.	3. RECIPIENT'S CATALOG NUMBER
4. TITLE (and Subtitle) Real Time Optical Data Modulator		5. TYPE OF REPORT & PERIOD COVERED Final Report Oct. 1973 - Nov. 1974
		6. PERFORMING ORG. REPORT NUMBER 105900-16-F
7. AUTHOR(s) I. Cindrich, G. Currie, C. Leonard and C. Aleksoff		8. CONTRACT OR GRANT NUMBER (s) F33615-74-C-1037
9. PERFORMING ORGANIZATION NAME AND ADDRESS Environmental Research Institute of Michigan P.O. Box 618 Ann Arbor, Michigan 48107		10. PROGRAM ELEMENT, PROJECT, TASK AREA & WORK UNIT NUMBERS
11. CONTROLLING OFFICE NAME AND ADDRESS Air Force Avionics Laboratory, AFAL/RWI Wright-Patterson Air Force Base Ohio 45433		12. REPORT DATE May 1975
		13. NUMBER OF PAGES 84
14. MONITORING AGENCY NAME AND ADDRESS (if different from Controlling Office)		15. SECURITY CLASS. (of this report) Unclassified
		15a DECLASSIFICATION / DOWNGRADING SCHEDULE
16. DISTRIBUTION STATEMENT (of this Report) Distribution limited to United States Government agencies only (Test and Evaluation); 22 April 1975. Other requests for this document must be referred to the Air Force Avionics Laboratory (AFAL/RWI), Wright-Patterson AFB, Ohio.		
17. DISTRIBUTION STATEMENT (of the abstract entered in Block 20, if different from Report)		
18. SUPPLEMENTARY NOTES		
19. KEY WORDS (Continue on reverse side if necessary and identify by block number) Recorder Thermoplastic Spatial Modulator Phase Modulator Data Transducer Optical Processing		
20. ABSTRACT (Continue on reverse side if necessary and identify by block number) Analysis of the performance characteristics of a laboratory model real-time thermoplastic optical data modulator was accomplished. De- sign of the modulator was performed in a previous program. Experiment- al data for bandwidth, dynamic range, spatial resolution and optical quality were obtained indicating a level of performance suitable for entry of wideband, high dynamic range data into a coherent optical pro- cessor or optical computer, or use of the modulator as a large screen display device.		

DD FORM 1 JAN 73 1473 EDITION OF 1 NOV 65 IS OBSOLETE

UNCLASSIFIED

SECURITY CLASSIFICATION OF THIS PAGE (When Data Entered)

UNCLASSIFIED

SECURITY CLASSIFICATION OF THIS PAGE (When Data Entered)

BLOCK #20.

The thermoplastic modulator provides electron beam writing on a reusable deformable thermoplastic surface giving a two-dimensional optical phase recording which may be rapidly erased upon command. Data written on the plastic surface may be retained for arbitrary lengths of time down to a minimum of about 100 milliseconds, prior to erasure. A 70 MHz temporal bandwidth, 30 c/mm spatial bandwidth and a recording dynamic range of at least 40 db were realized. The experimental modulator system was designed in two configurations which differed mainly in the thermoplastic recording surface geometry. These two implementations were a fixed plate and a rotated disc recording arrangement. The fixed plate system provides a 5 inch diameter substrate on which central 3 inch diameter area is used for recording. The rotated disc system utilizes a 15 inch diameter substrate which is mechanically rotated past the repetitively line scanned electron beam. The thermoplastic recording region lies in a band between radii of 2 inches and 6.5 inches. Various data formats are provided by electronic scan control of the writing electron beam in addition to the mechanical rotation of the recording surface in the case of the rotated disc system. Optical quality of the recording medium of better than one fourth wavelength flatness over a one inch region is achieved using materials and thermoplastic coating techniques developed in this program.

UNCLASSIFIED

SECURITY CLASSIFICATION OF THIS PAGE (When Data Entered)

FOREWORD

The program reported here was accomplished in the Electro-Optics Section, Radar and Optics Division of the Environmental Research Institute of Michigan. This effort was sponsored by the Air Force Avionics Laboratory, Contract F33615-74-C-1037. with D. Flannery the Air Force Project Engineer. The work was accomplished in the period October 1973 through November 1974. Principal Investigator at ERIM was I. Cindrich. Additional staff members contributing were G. Currie, G. Orbits, R. Salmer, and D. Wertz. The ERIM number for this report is 105900-16-F.

TABLE OF CONTENTS

1.	Introduction	1
2.	System Configuration	4
3.	Data Readout	8
4.	Performance Characteristics.	12
5.	Thermoplastic and Substrate Properties	20
6.	Recording Format	32
6.1	Rectangular Format Data	35
6.2	Polar Format Data	38
6.3	Experimental Analysis of Polar Data	43
6.4	Unsynchronized Modulation Coupling.	53
6.5	Further Derivation of Polar Data Transform.	56
6.6	Optical Rectification	80
7.	Conclusions and Recommendations.	81
8.	References	82

LIST OF ILLUSTRATIONS

1.	Data Storage by Thermoplastic Deformation.....	3
2.	Data Readout for Optical Processing.....	3
3.	Thermoplastic Modulator-Fixed Plate Configuration.....	5
4.	Thermoplastic Modulator - Rotating Disc Configuration...	5
5.	Bessel Function of the First Kind.....	10
6.	Experimental Real Time Optical Processing.....	12
7.	Amplitude Modulation Transfer Function for Several Different Writing Beam Sweep Speeds.....	15
8.	System Writing Sensitivity, Second Harmonic and Noise Data.....	16
9.	Single Frequency (Spot) Distribution for Circular and Square Input Apertures.....	17
10.	Microscopic Scan of Frequency Plane for Circular Input Aperture.....	18
11.	Microscopic Scan of Frequency Plane for Square Input Aperture.....	19
12.	Thermoplastic Substrates.....	21
13.	Coating Table and Forms.....	22
14.	Thermoplastic Application.....	24
15.	Coating Form Enclosure.....	25
16.	Coating Tools.....	28
17.	Composite Interferogram of TP Coated 15" Disc.....	30
18.	Interferogram of TP Coated 5" Plate.....	31
19.	Coordinate Geometry.....	32
20.	Input Signal Format.....	33
21.	Polar Recording.....	44
22.	Frequency Plane for Input Aperture A.....	45

23.	Frequency Plane for Input Aperture B.....	46
24.	Frequency Plane Polar Parameters.....	48
25.	Frequency Plane - Two Input Signals, Small Aperture.....	50
26.	Frequency Plane - Two Input Signals, Increased Radial Aperture.....	51
27.	Two Input Signals, Large Aperture.....	52
28.	Radial Line Spectrum.....	58
29.	Circular Point Set Spectrum.....	60
30.	The Function $\text{Sinc}_N(\frac{k}{p})$	65
31.	The Function $\text{III}(\frac{A}{B})\text{rect}(\frac{A}{NB}) * \text{III}(A)$	72
32.	Frequency Plane Structure.....	75

SUMMARY

Analysis of the performance characteristics of a laboratory model real-time thermoplastic optical data modulator was accomplished. Design of the modulator was performed in a previous program. Experimental data for bandwidth, dynamic range, spatial resolution and optical quality were obtained indicating a level of performance suitable for entry of wide-band, high dynamic range data into a coherent optical processor or optical computer, or use of the modulator as a large screen display device.

The thermoplastic modulator provides electron beam writing on a reusable deformable thermoplastic surface giving a two-dimensional optical phase recording which may be rapidly erased upon command. Data written on the plastic surface may be retained for arbitrary lengths of time down to a minimum of about 100 milliseconds, prior to erasure. A 70 MHz temporal bandwidth, 30 c/mm spatial bandwidth and a recording dynamic range of at least 40 db were realized. The experimental modulator system was designed in two configurations which differed mainly in the thermoplastic recording surface geometry. These two implementations were a fixed plate and a rotated disc recording arrangement. The fixed plate system provides a 5 inch diameter substrate on which central 3 inch diameter area is used for recording. The rotated disc system utilizes a 15 inch diameter substrate which is mechanically rotated past the repetitively line scanned electron beam. The thermoplastic recording region lies in a band between radii of 2 inches and 6.5 inches. Various data formats are provided by electronic scan control of the writing electron beam in addition to the mechanical rotation of the recording surface in the case of the rotated disc system. Optical quality of the recording medium of better than one-fourth wavelength flatness over a one inch region is achieved using materials and thermoplastic coating techniques developed in this program.

1
INTRODUCTION

A thermoplastic modulator which provides real-time insertion of data to the input of a coherent optical processing channel has been designed and its performance properties evaluated. The initial fabrication of components for this experimental system was accomplished in a previous program.¹

Coherent optical data processing systems offer excellent and often unique performance features. The use of coherent optical systems of course requires entry of the data to be processed in a two-dimensional spatial format at the input plane of the processing optics. Where the signal to be processed is a time varying voltage, a recording device (data modulator or transducer) is required that will, generally, be comprised of a writing beam that is modulated in proportion to the signal to be recorded, and, a recording medium on which the beam writes in the desired spatial format. For optical processing the recorded data is illuminated with a coherent light beam, the recording causing a variation in either the phase or amplitude of the illuminating beam depending upon the type of recording medium employed. This spatially modulated light beam is then processed using lenses and spatial filters to provide the data processing or display functions of interest.

There are several concepts potentially available for application as a near real-time data recorder² having high optical quality and a reusable recording medium. The recording concepts may be categorized generally as to type of writing beam and recording material used. Typically either an electron beam or light beam is used for writing. The list of recording medium candidates, which is somewhat dependent on the type of writing beam used, includes deformable plastics, deformable membranes, variable scattering in liquid crystals or ferroelectric ceramics, variation of optical transmittance in cathodochromics or photo-

chromics, and, variation of induced birefringence in several possible electro-optic materials.

The use of a thermoplastic data modulator employing an electron writing beam offers considerable flexibility in design of the beam scanning provisions particularly for the case of a two-dimensional scan format. In addition, modulation of the writing beam in correspondence with the input signal to be recorded is comparatively straightforward for bandwidths to at least one hundred megahertz and can be accomplished to considerably greater bandwidths with special electron beam electrode design. These factors provide a natural motivation for use of a real-time modulator which employs an electron beam. The suitability of the thermoplastic recording material is governed by such performance factors as recording quality and sensitivity, optical quality, optical diffraction efficiency and recycle life. Thermoplastic offers the potential for good recording sensitivity and quality with optical readout allowable over a wide range of wavelengths and at comparatively good efficiency. A deformable thermoplastic has been developed as a near real-time recording medium with good optical quality and thickness uniformity. Data recording is accomplished by causing surface deformations of a thin thermoplastic layer as depicted in Figure 1. The deformations are caused by the electrostatic force of the charge deposited by the writing electron beam when the plastic is sufficiently softened by raising its temperature. A further increase in temperature causes the recorded data to erase by allowing the surface charge to be conducted through the plastic with surface tension forces then acting to smooth the surface. The readout laser beam becomes phase modulated in correspondence with the recorded variations in thickness of the deformed plastic as depicted in the sketch of Figure 2.

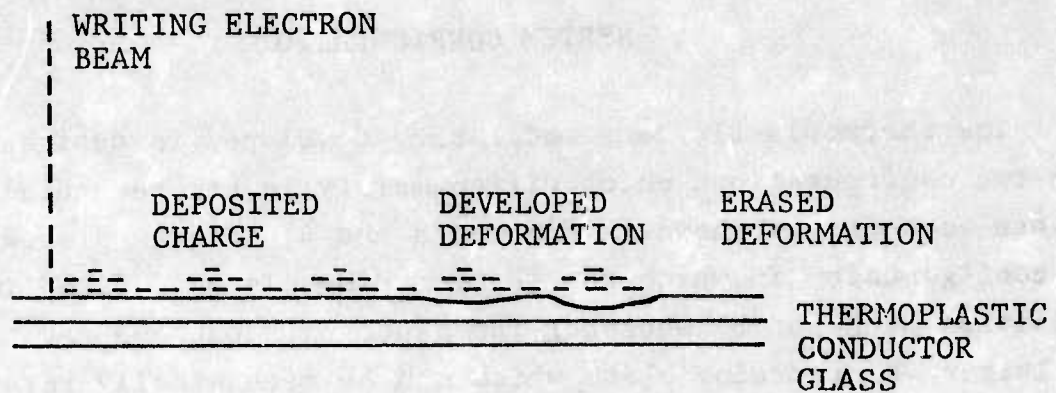


FIGURE 1. DATA STORAGE BY THERMOPLASTIC DEFORMATION

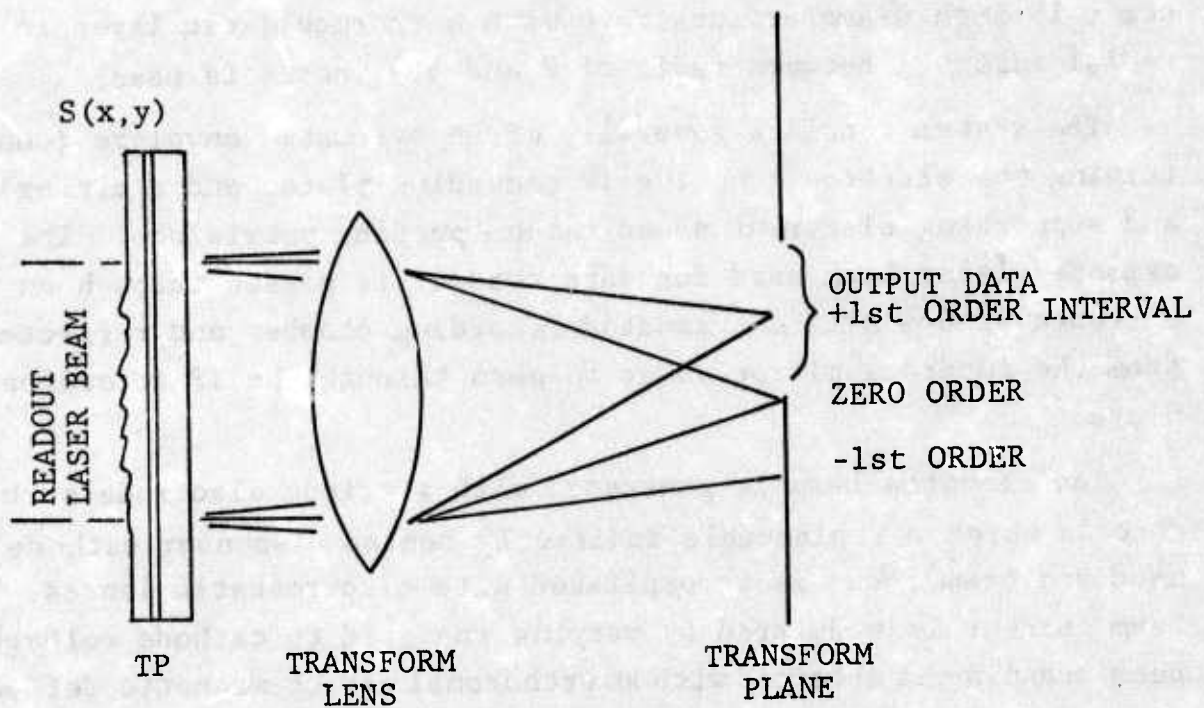


FIGURE 2. DATA READOUT FOR OPTICAL PROCESSING

2 SYSTEM CONFIGURATION

The thermoplastic data modulator developed is designed in two configurations which differ mainly in the recording plate geometry as shown in Figures 3 and 4. Figure 3 shows a configuration in which the TP recording plate is fixed in position much as the phosphor faceplate of a cathode ray tube. A larger TP recording plate which can be mechanically rotated either continuously or incrementally is used in the second configuration shown in Figure 4. At present the fixed plate system makes use of a 5 inch diameter fused silica substrate with a transparent gold coating over which the thermoplastic is coated in the central 4 inch diameter region. In the rotated plate system a 15 inch diameter substrate with a thermoplastic layer in a radial interval between radii of 2 and 6.5 inches is used.

The system consists generally of an evacuated envelope (containing the electron gun, the TP recording plate, and a mirror) and supporting electronics and vacuum pumping provisions. The expanded laser beam used for data readout is passed through an entrance window of the evacuated recording chamber and reflected from the internal mirror so as to pass through the TP recording plate.

The electron beam is generated with a triode electrode structure in which a replaceable indirectly heated dispenser cathode is used and beam focus is accomplished with electrostatic lenses. Beam current is modulated by varying the grid to cathode voltage. Beam scanning is obtained with an orthogonal set of magnetic deflection coils. A 6 KV beam voltage with beam current up to about 1 μ a is used.

In the fixed plate system the writing beam can be electronically scanned in a rectangular raster or a polar raster format. With the rotating disc configuration the electron beam scans repetitively over a single line as the disc rotates past it or in a sequence of small rasters.

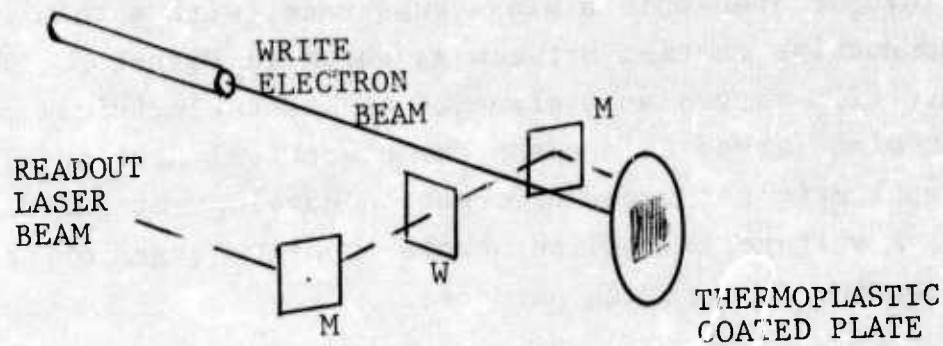


FIGURE 3. THERMOELASTIC MODULATOR - FIXED PLATE CONFIGURATION

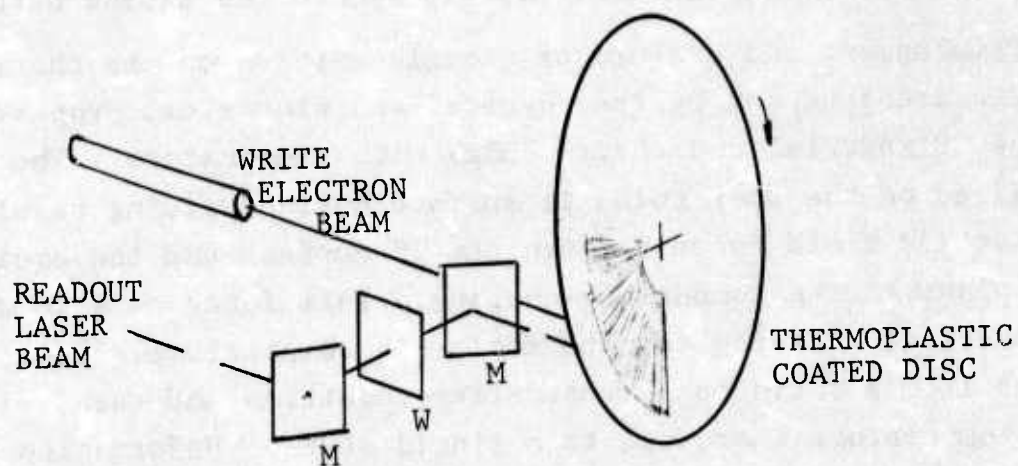


FIGURE 4. THERMOELASTIC MODULATOR - ROTATING DISC CONFIGURATION

The storage medium is comprised of a thin ($\approx 6 \mu\text{m}$) thermoplastic layer coated onto a glass substrate, with a thin transparent conductive coating between as shown in Figure 1. The conductive film serves as a plane of constant electrical potential. It also serves as a means for electrical heating (I^2R) of the thermoplastic for rapid deformation development and data erasure. A voltage is applied across opposite edges of the conductive coating for heating purposes.

Thermoplastic can be operated either in a continuous develop-erase mode or a pulsed develop-erase mode. In the continuous mode the TP temperature is held at a level which allows fairly rapid development of recorded deformations and slightly slower erasure of the recorded data. Some variation of develop and erase time constants is possible depending upon the material used and the operating temperature selected. For a temperature of 60°C the system described here provides deformation development in about 5 seconds and a 60 second erasure. Pulsed control of the TP temperature allows development in less than one second after which the recorded data can be retained until application of an erase pulse which will rapidly remove the stored data.

Development and erasure of signals written on the thermoplastic are governed by the physical and electrical properties of the TP material and their change with temperature. The charge deposited on the thermoplastic surface during writing results in an electric field force between the TP surface and the equipotential plane at the conductive coating. This force acts to deform the surface. Raising the thermoplastic temperature allows it to change from a solid to a rubber-like condition and then, with further temperature increase, to a liquid state. Deformation development can occur while the thermoplastic is in either of these softened states. The depth of the deformation will be limited by counteractive surface tension and viscoelastic forces. Erasure of signal deformations occurs when the surface charge is removed and the thermoplastic temperature is elevated so the plastic

reaches a non-solid state and can be re-distributed so as to form a smooth surface in response to the surface tension and viscoelastic restoring forces. In erasure, the written surface charge is removed by electrical conduction through the plastic to the conductive layer when the TP resistance is lowered by heating.

3
DATA READOUT

Data written on the thermoplastic is read out with a laser beam expanded to illuminate the area over which stored signals of interest appear, as shown in Figure 2. The sketch shows readout by transmission. (Reflective methods are also possible). The basic properties of optical readout of the phase data is discussed in this section with a more detailed description relating to recording format given later in Section 6.

In rectangular coordinates x, y the complex transmittance of the thermoplastic plate can be written as $T(x,y)e^{j\alpha(x,y)}$ where T is the amplitude transmittance and α the phase shift caused by the plastic and substrate. Given an illuminating beam having a wavefront with uniform phase and constant amplitude over an aperture $A(x,y)$, the emergent beam $S(x,y)$ at the output side of the glass substrate will be of the form

$$S(x,y) = A(x,y) T(x,y)e^{j\alpha(x,y)}$$

The amplitude transmittance will normally be constant, i.e., $T(x,y) = T_0$. Phase shift at the optical wavelength can be written as $\alpha(x,y) = [2\pi(n - 1)/\lambda]d(x,y) + \beta$, where d is surface deformation depth, n is the index of refraction of the thermoplastic and β is a phase shift caused by materials other than the thermoplastic, i.e., substrate and conductive coating. Thus the emergent phase-modulated readout beam is written as

$$S(x,y) = A(x,y)T_0e^{j\left[\frac{2\pi(n-1)}{\lambda}d(x,y)\right]}e^{j\beta}$$

For example, consider the deformation d to be a one-dimensional sinusoid of spatial frequency ω_x

$$d = D_0 + D \sin \omega_x x$$

as indicated in Figure 2. Considering the x variation only for convenience, the expression for the phase modulated readout beam S can be written as

$$S(x) = A(x) T_0 \sum_{m=-\infty}^{\infty} J_m \left[\frac{2\pi(n-1)}{\lambda} D \right] \exp jm\omega_x x$$

where we have ignored constant phase terms and $J_m[]$ is a Bessel function of the first kind, order m . An example of the amplitude variation given by the Bessel functions is given in the data of Figure 5. The indexing variable m takes on all integer values. Thus, there are plane waves $e^{jm\omega_x x}$ emanating from the modulator; each has a field amplitude $J_m \left\{ \left[\frac{2\pi(n-1)}{\lambda} \right] D \right\}$ and all come through the aperture $A(x)$.

If the transducer output is Fourier transformed optically as depicted in Figure 2, the Fourier transform lens will focus each of the plane waves $e^{jm\omega_x x}$ into a small spot of light at the output transform plane of the lens. In this example each spot of light will have a shape or spatial distribution dependent on the size and shape of the data aperture or apodization within the aperture $A(x)$. For a uniformly illuminated round aperture the familiar Airy disc distribution, $\left| \frac{J_1[]}{[]} \right|^2$, is obtained. The peak value of the light intensity of the focused spot will be proportional to $J_m^2 \{ [2\pi(n-1)/\lambda] D \}$ and thus depends upon the depth D of the sinusoidal deformation in the thermoplastic. The distance of a spot from the zero order position will be directly proportional to the

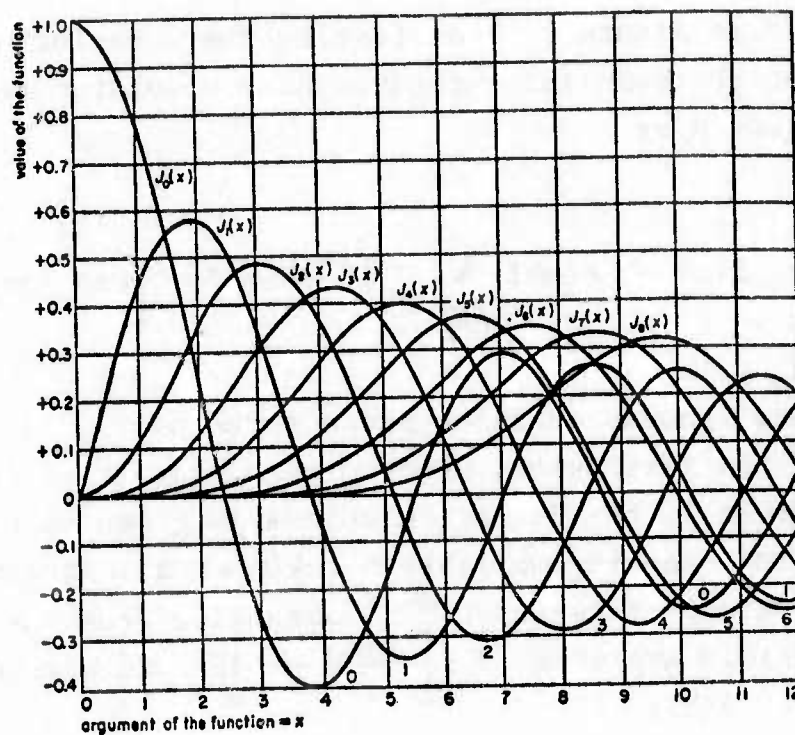


FIGURE 5. BESSEL FUNCTIONS OF THE FIRST KIND

spatial frequency ω_x in the plane wave expression $e^{jm\omega_x x}$ and its angular location will be on a line orthogonal to the input grating lines. Only data corresponding to one of the first orders ($m = \pm 1$) are usually used for optical processing. The deformation depth D is then chosen to optimize the performance of the transducer in terms of linearity and diffraction efficiency. Diffraction efficiency for first order data is taken as the ratio $J_1^2[]$ to $\sum_m J_m^2[]$.

While phase modulation of the readout beam provides greater diffraction efficiency than other modulator concepts it will typically be held to a few per cent to obtain linear operation and to limit higher order diffraction and intermodulation products.

4
PERFORMANCE CHARACTERISTICS

Several system as well as component characteristics have been investigated and some of the results will be reviewed in this section.

System performance was tested while using the fixed plate modulator in an optical Fourier transform data processing mode of operation as depicted in Figure 6. Data recorded as thermo-plastic surface deformations was illuminated with an expanded and collimated HeNe laser beam. The phase modulated light beam wavefront emergent from the TP layer is Fourier transformed by lenses as shown in Figure 6. The output light distribution at the spatial frequency (Fourier transform) plane was examined as a function of the input voltage used to modulate the current of the electron beam and several operating parameters. Beam current was modulated relative to a bias level set by a bias voltage at the modulation electrodes of the electron gun.

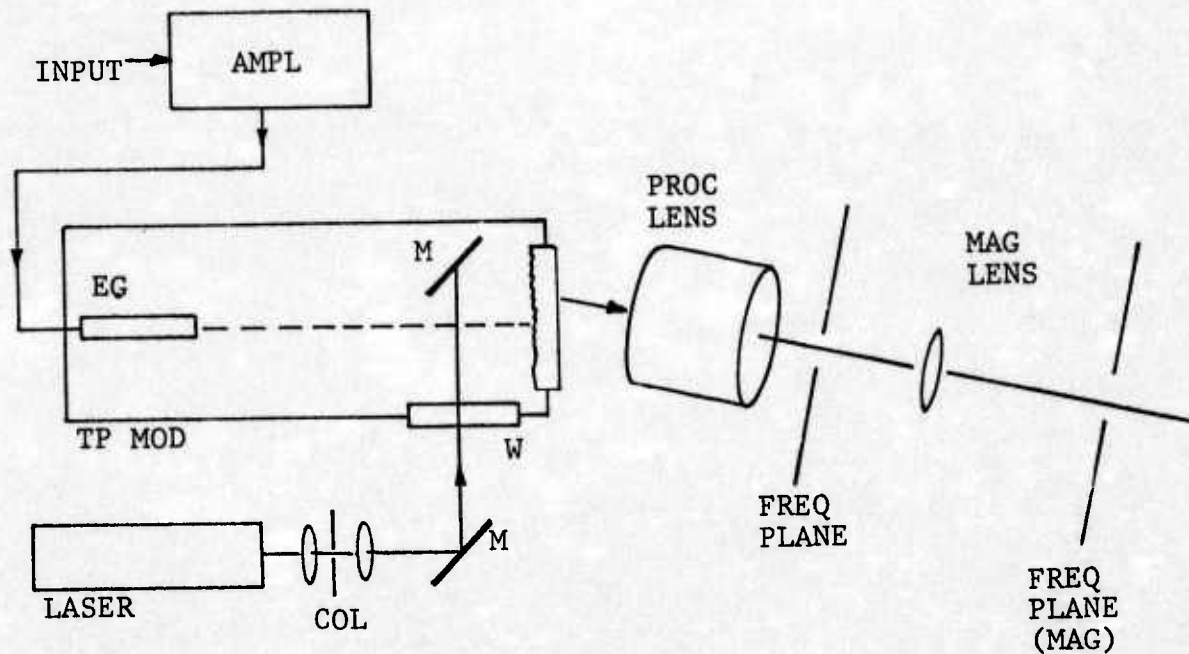


FIGURE 6. EXPERIMENTAL REAL-TIME OPTICAL PROCESSING

The amplitude modulation transfer function (AMTF) is described by the data of Figure 7. Shown is the relative amplitude of the peak value of the first order diffracted spot of light in the spatial frequency plane as a function of the frequency of the input signal used to modulate writing beam current. Light amplitude was computed as the square root of measured light intensity. The data was taken at approximately 2, 5 and 10 MHz increments for curves A, B and C, respectively. The AMTF curves corresponding to several different values of writing beam sweep speed are given. Though not shown in the data, a recorded response was realizable up to frequencies of 90 MHz when using the highest sweep speed. A temporal bandwidth of about 70 MHz at the 5 per cent response points is achieved when using the highest speed. As sweep speed is reduced the AMTF is scaled toward lower frequencies and at a higher sweep speed a greater bandwidth can be realized to the extent that sufficient beam current is available for exposure of the thermoplastic.

Relative gain and dynamic range data for the system can be seen in Figure 8. System gain is given by the plot of relative amplitude of the peak value of the first order diffracted light spot in the spatial frequency plane as a function of the peak-to-peak value of the input sinusoidal voltage used to modulate the writing electron beam. Frequency of the input voltage was held constant at either 10 MHz or 20 MHz when performing this test. The amplitude of the peak value for the noise background and of the second order diffracted light at the spatial frequency plane is also given. As shown a recorded signal variation for inputs from 0.1 to at least 18 volts is achievable. The ratio of maximum output (22) to RMS noise (0.2) for the modulator was 110 or a dynamic range of 40.8 db.

Diffraction efficiency, taken as the ratio of first order to zero order diffracted light intensity, is about 3 per cent for the recording of a 15 volt peak-to-peak input sinusoidal voltage.

An indication of the quality of the diffracted light spot in the spatial frequency plane is shown by the photographs of Figure 9. The light distribution shown in Figure 9a and 9b is caused by a 30

MHz recording (sine wave grating) within a square illumination aperture at the thermoplastic surface. Figures 9c and 9d are diffraction patterns obtained with no recorded data (zero frequency) with a square input aperture and Figures 9e and 9f are similar data obtained when using a circular input aperture. Good recording medium and recorded data quality are indicated by the light distributions shown in Figure 9 which correspond to nearly diffraction limited performance for data apertures up to at least an inch.

A microscopic scan of the diffraction pattern intensity distributions for the circular and square apertures is shown in Figures 10 and 11 which indicate good correspondence to theoretically predictable results in mainlobe and sidelobe relationships. The left and right sidelobes are nonsymmetric in peak levels which is believed caused by a slight nonuniformity in coating thickness. The magnified frequency plane spots were scanned with a photometer having a 10 μm circular scanning aperture. The photometer output was amplified with a logarithmic amplifier and recorded on an X-Y chart recorder to obtain the data shown in these figures. The vertical (intensity) scale is logarithmic with approximately 0.37 dB per smallest division. The horizontal (distance) scale is 1.2 μm per smallest division for the 1" aperture data and about 1.6 μm per division for the 1/2" aperture data when observed at the output (frequency) plane of a diffraction limited 12" focal length lense. The intensity level baseline is caused by the photometer noise level. The single frequency spot distributions shown in these figures correspond to the theoretical diffraction limited distributions to within about 15 percent indicating good optical quality and writing fidelity.

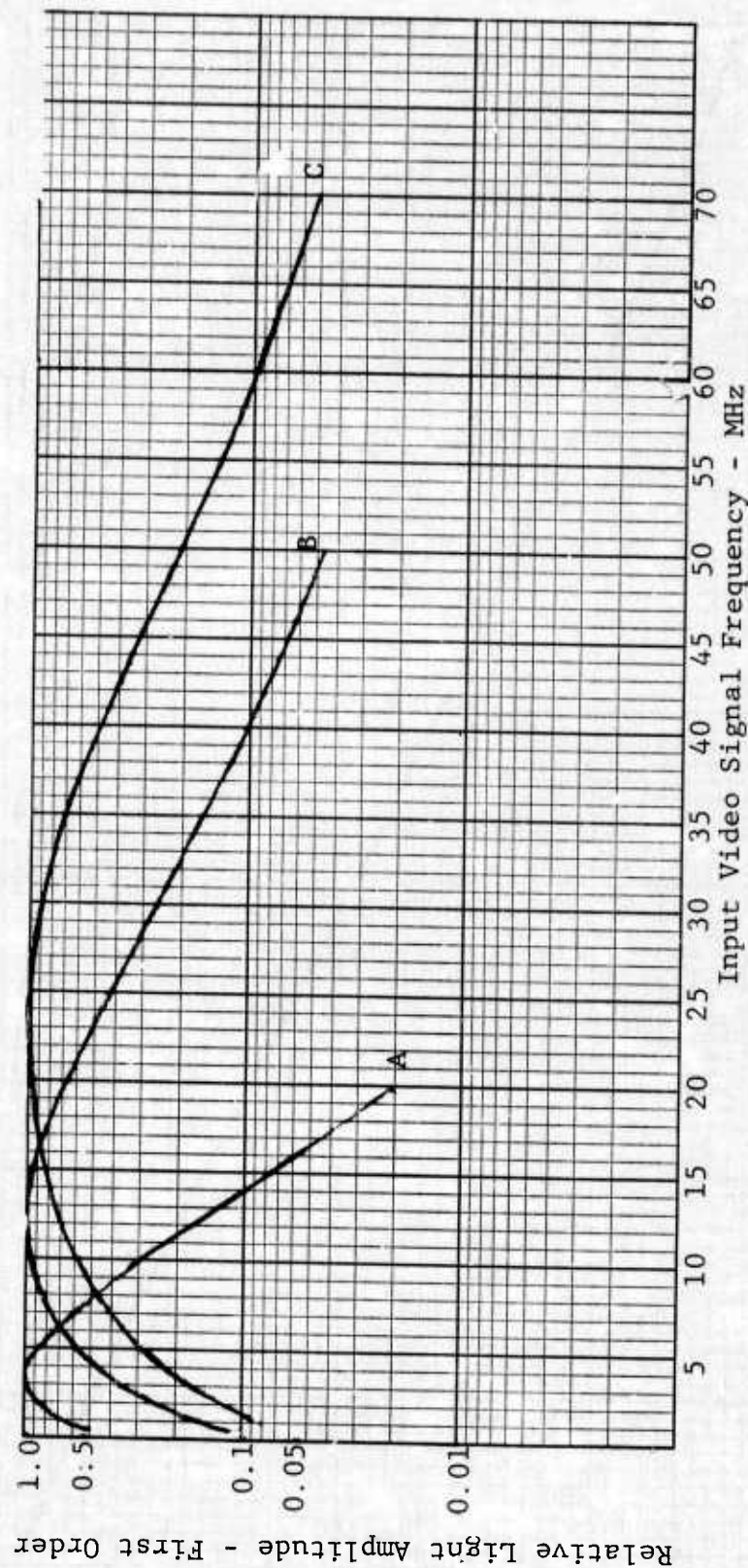


FIGURE 7. AMPLITUDE MODULATION TRANSFER FUNCTION FOR SEVERAL DIFFERENT WRITING BEAM SWEEP SPEEDS. A - 10 μ s/inch, B - 20 μ s/inch, C - 80 μ s/inch.

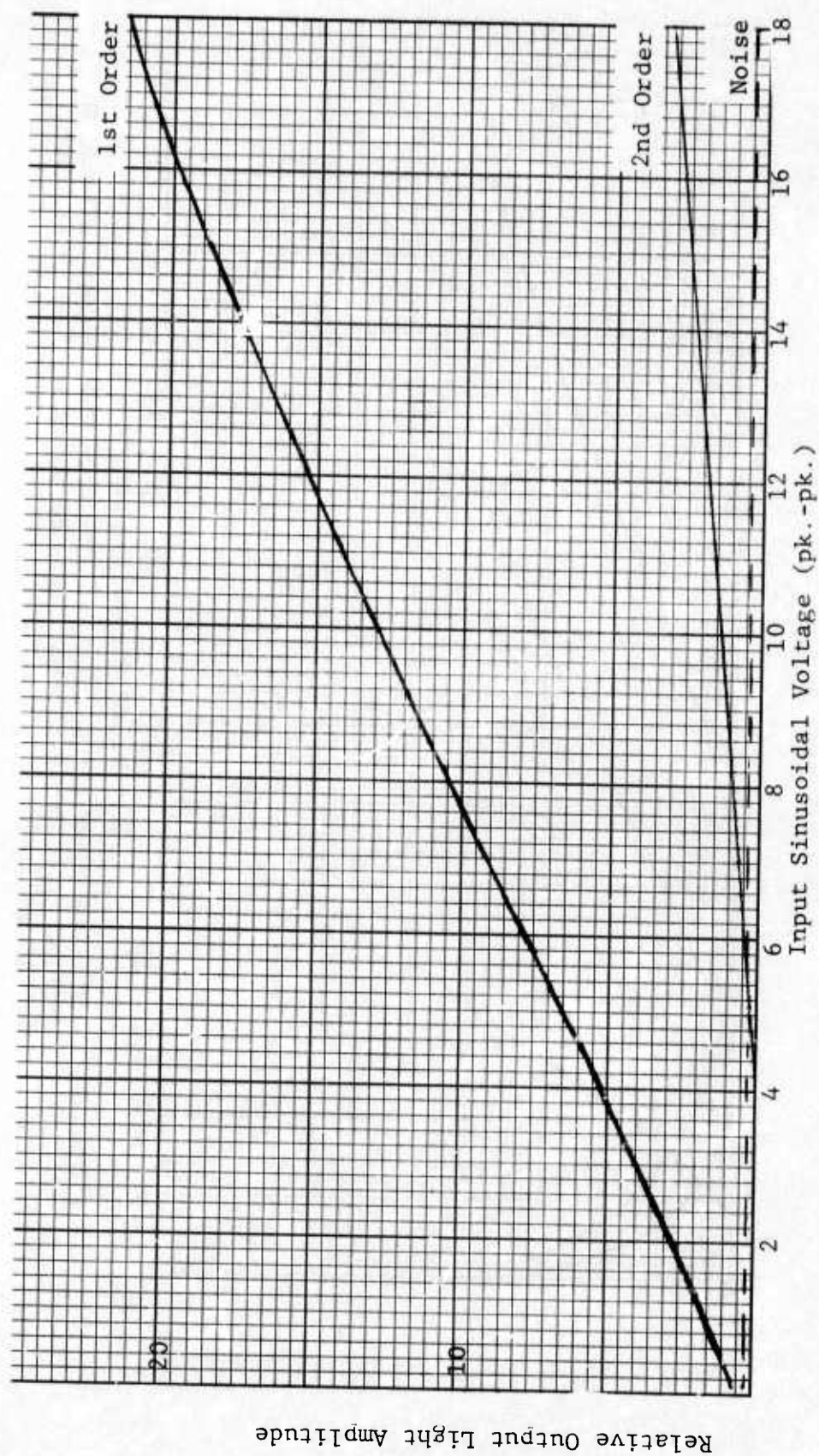
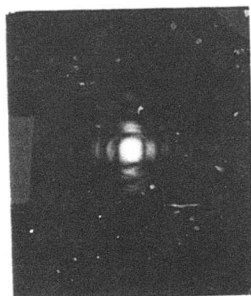
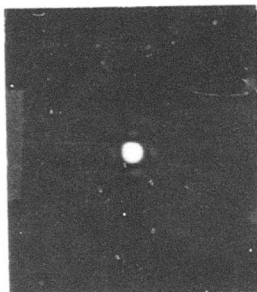


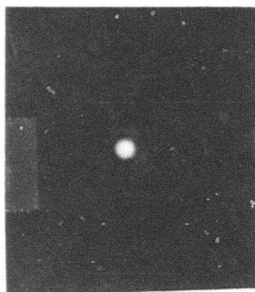
FIGURE 8. SYSTEM WRITING SENSITIVITY, SECOND HARMONIC AND NOISE DATA



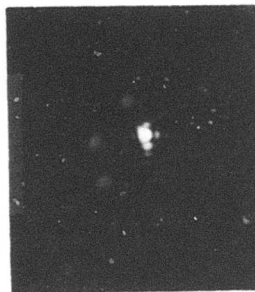
(a) 30 MHz
 $\frac{1}{2}$ " Aper-S



(c) Zero Frequency
 $\frac{1}{2}$ " Aper-S



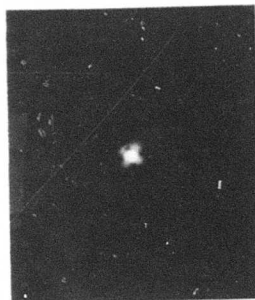
(e) Zero Frequency
 $\frac{1}{2}$ " Aper-C



(b) 30 MHz
1" Aper-S

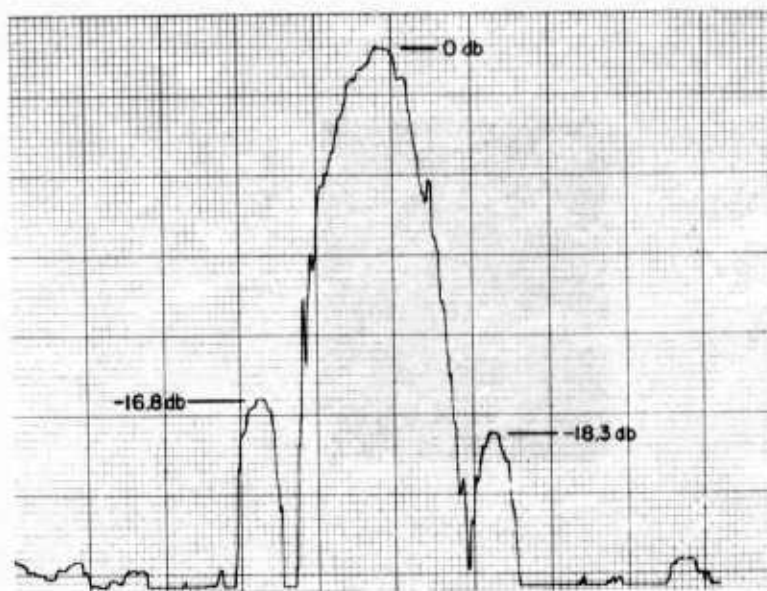


(d) Zero Frequency
1" Aper-S

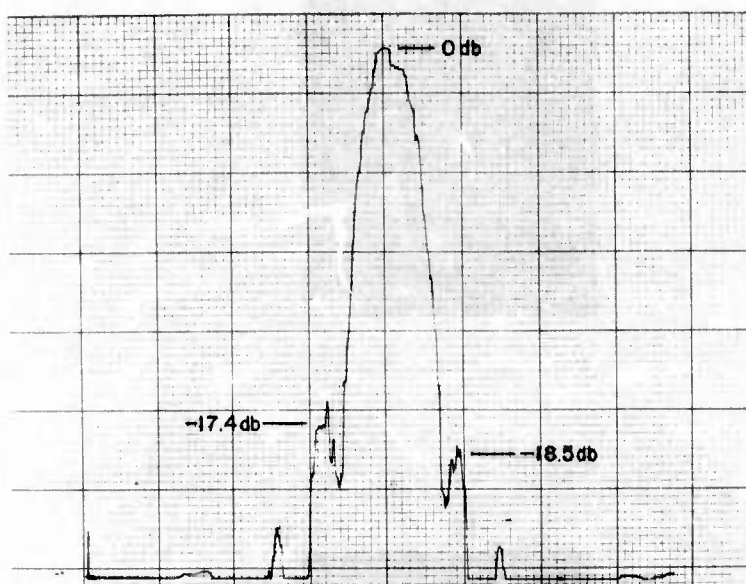


(f) Zero Frequency
1" Aper-C

FIGURE 9. SINGLE FREQUENCY SPOT DISTRIBUTION (C-Circular Aperture,
S- Square Aperture)

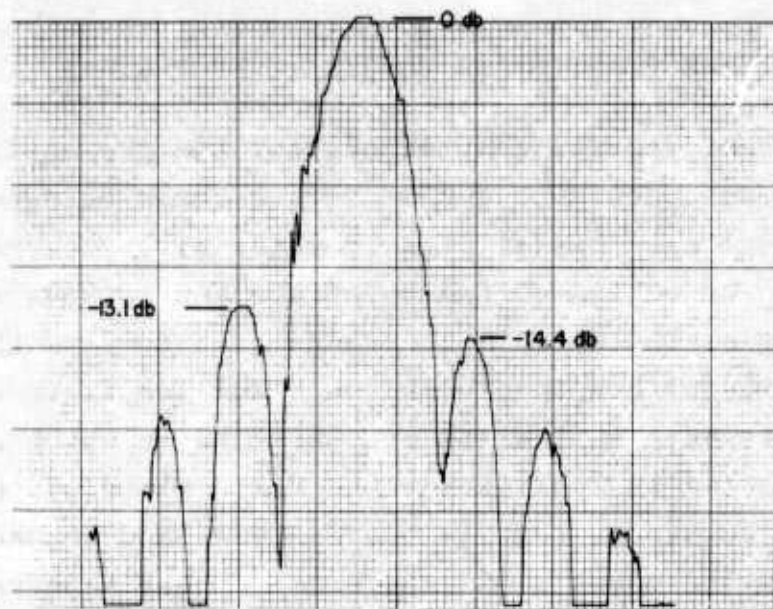


1/2" Aperture

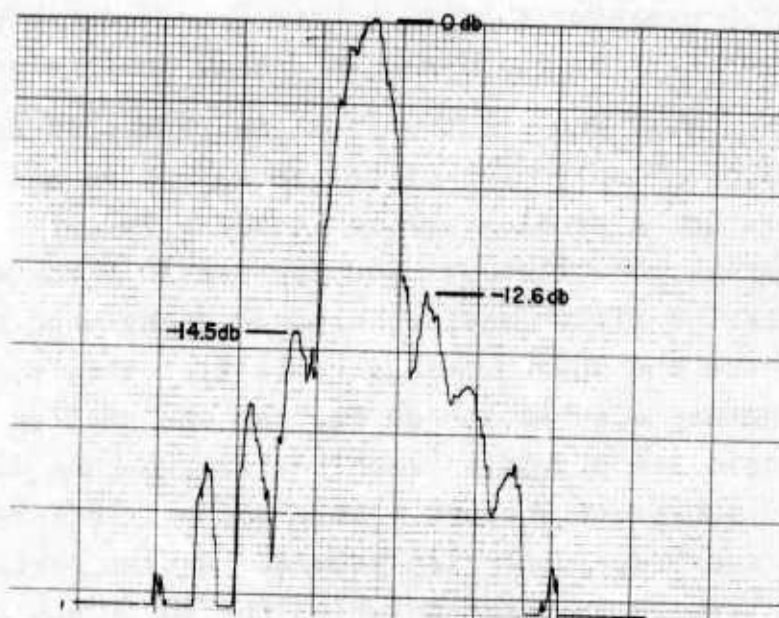


1" Aperture

FIGURE 10. MICROSCOPIC SCAN OF FREQUENCY PLANE FOR CIRCULAR INPUT APERTURE



$\frac{1}{2}$ " Aperture



1" Aperture

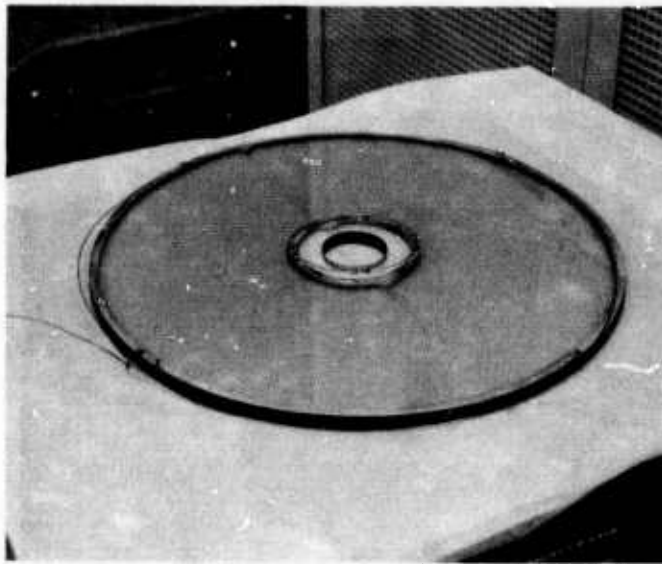
FIGURE 11. MICROSCOPIC SCAN OF FREQUENCY PLANE FOR SQUARE INPUT APERTURE

5
THERMOPLASTIC AND SUBSTRATE PROPERTIES

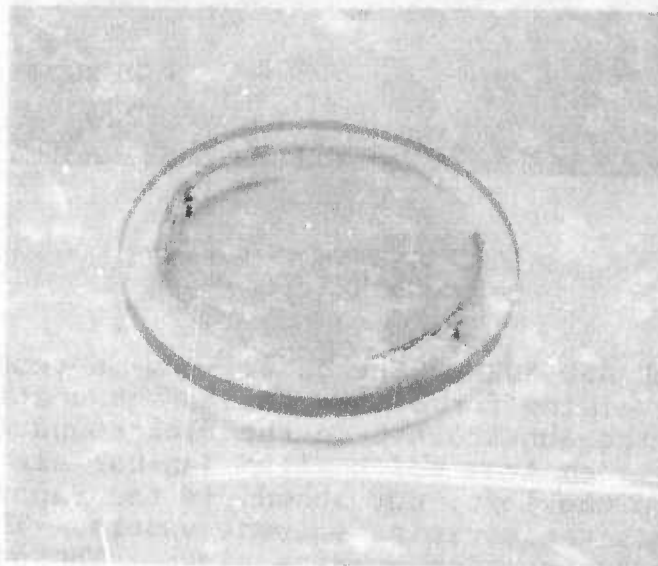
Development of fabrication methods for the thermoplastic recording medium was continued during this program using only one of several potentially useful plastic materials. The main emphasis has been on design of the substrate and methods for application of the plastic layer in the range of 5 to 7 μ m thick with a high uniformity of coating thickness. Two substrate sizes have been developed: a 5" diameter substrate on which a 4" diameter TP coating is applied for the fixed plate system; and a 15" diameter substrate that is coated in a band between radii of 2" and 6.5" for the rotating disc system. These substrates are constructed from 3/8 thick optical quality fused silica with a transparent gold conductive film and silver electrode strips for electrical contact as shown in Figure 12. The coating methods developed for the 5" diameter substrate have been described previously¹ and only the large disc is discussed in detail in this section.

With the large disc many of the problems that occurred with the previously developed 5" diameter plate are magnified and other factors that were not a problem before became a factor. For a satisfactory coating, good flatness and low particle contamination are required. Let us first consider producing the best flatness. To improve flatness the substrate has to be flat itself. Due to manufacturing factors a substrate as flat as the smaller discs is difficult to obtain. A precision granite flat, Figure 13, was implemented as the substrate support. This not only offered overall support for the substrate, but also provided a flat surface for the glass to conform to in cases in which the substrate was slightly warped in some fashion. The substrate can be leveled to at least 10 seconds of arc.

As with the smaller coatings a certain solvent and solvent layer thickness are required with a given thermoplastic. These parameters may vary with thermoplastic, but appear to be independent of coating



15" Diameter Disc



5" Diameter Disc

FIGURE 12. THERMOPLASTIC SUBSTRATES



FIGURE 13. COATING TABLE AND FORMS (The outer form is removed showing the inner retaining forms that define the coating layer boundary on the substrate. In the background is the front of the clean room from which clean laminar air flows horizontally. To the left, not shown, is the vapor hood, which collects the escaping solvent vapors. The form is sitting on a precision granite plate. The plate is leveled by four screws (40 threads/inch) at the bottom of the support stands).

area. The thermoplastic solution used, due to a property of the thermoplastic, did not readily wet the surface but had to be spread over the area with a stir rod, Figure 14. First, the solution was applied more or less uniformly about the circumference of the annulus being coated. A stir rod was used to move the solution layer to the boundaries. This joining was done last in order to minimize the quantity of solution captured by the edge. The spreading of the solution by the stir rod required a technique that applies the solution rapidly but uniformly. It was found that the size of the stir rod was important. A rod too small (in terms of the width of the rod which interfaces with the solution) increased the application time unduly. A rod too wide left an area behind the center of the rod where the solution layer was too thin. The rod would appear to drag the liquid rather than push it. The rod should be moved rapidly around the coating area without overconcern as to how thick the solution layer is. Where the layer is too thin such as occurred with the extra wide stir rod, the solution layer will break through after several seconds so that the area must be wetted again from neighboring areas. Holding the solution layer in a quiet state after spreading and before drying helps insure good flatness.

During the spreading period there is a certain amount of solvent evaporation. This is undesirable in that when the solution layer is in the form of a large sessile drop the greatest evaporation occurs near the edge, since the vapors readily diffuse to the surrounding uncoated area. Hence, nonuniformities in concentration will be produced. Then, even with an initially smooth solution layer, the final surface will not be flat. To reduce the evaporation, the surrounding atmosphere is saturated with the solvent vapor. In addition, the circulation of air is reduced by a double enclosure surrounding the solution layer. First is the metal form which also acts to dam the solution layer, Figure 13, and then a surrounding fiberglass-epoxy enclosure that reduces the circulation into the first form, Figure 15.

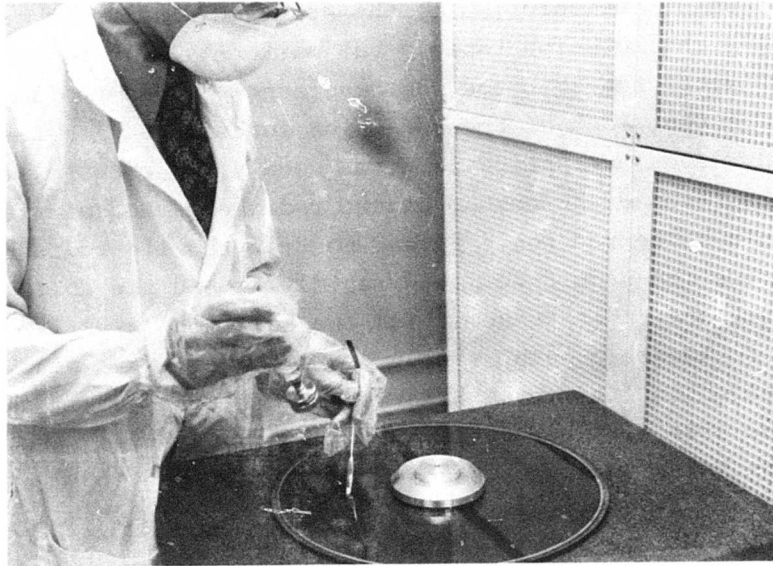


FIGURE 14. THERMOPLASTIC APPLICATION (OUTER RETAINING FORM REMOVED).



FIGURE 15. COATING FORM ENCLOSURE

The flatness of the solution layer can be checked by observing the reflections of the overhead lights. When it appears that the coating is sufficiently flat so that no more breakthrough will occur, the lids of both forms are put on for about 20 minutes. Next, the coating is allowed about two hours to dry. During that period the rate of circulation is gradually increased. If the drying period is too long a radial wedge can be introduced into the coating. This occurs because, typically, the outer edge tends to evaporate more quickly so the solution drains from inside causing the solution layer on the inside to become thin with the possibility of breakthrough. The latter effect would occur subsequent to the occurrence of a wedge if it occurs at all, and would require a new start in the procedure. This possibility is diminished by loading the outer form with solvent in a trough along the wall which saturated the air with vapor. Having a configuration in which there is even evaporation is essential but it is hard to maintain for a long time interval. The slower the evaporation and circulation the more likely will be a vapor gradient. These problems were reduced by the above mentioned addition of solvent vapor and were further diminished by increasing the circulation gradually as the solution layer becomes concentrated and more viscous. The sequence used to realize the increased circulation is first, the lid of the outer form is placed ajar; second, the same lid removed. The latter must be done at the right time and with care in order that no solvent is dropped on the coating. The TP solution along the edge should not be so dry that strings of TP are pulled up and fall onto the coating, or worse, that the form is frozen onto the substrate. On the other hand, it should not be so wet that the TP solution drips onto the coating.

Problems with particle contamination have been considered and much progress has been made. The acetone-acetate method whereby acetone is applied and then an acetate sheet (the acetate is partially dissolved and surrounds and traps the particles) which worked on the smaller discs was not as satisfactory on the large disc. With the large disc, the application time increased and during that time the ace-

tate swelled sufficiently to make a smooth, bubble free acetate layer nearly impossible. Changing to methyl-ethyl-ketone improved the results; however, the acetate would separate from the substrate before completely drying. The hole in the middle of the large disc substrate and the adjacent electrode made cleaning more difficult. The acetate cleaning technique cannot be extended over the central area (outside of the region to be coated) because of the vertical extension of the electrodes, particularly at the attachment points. The central area is not as clean as the surrounding area and contamination may result if particles become detached. Having no success with the acetate sheet method a series of wash and soft-wipe procedures was used.

Filtering the quantity of solution required for coating the large disc in a short time (to minimize the evaporation of the solvent during application) created problems. The high pressure syringe caused some solution to leak from the Luer lock of the syringe filter connection. Other lower pressure Teflon filters were used but these had produced even worse leakage problems within the filter holder. The presence of a leak did not necessarily contaminate the coating if precautions were taken; however, control of a leak diverted attention from the coating effort. Recently, new nylon filters were tried on smaller coatings and problems with leaks and high back pressure were corrected, Figure 16.

With a smaller coating, the intrusion by the coating apparatus was shorter in time, and less extended physically requiring that only the stir rod and the filter apparatus enter into the still region above the solution layer. With the larger coating the syringe, the hands, and arms of the coater were directly in that region. Care was taken so that these additions do not introduce particle matter. Precautions included use of a filter mask over the nose and mouth, nylon cap and a coat with disposable gloves taped to the sleeves of the coat, Figure 14.. The fact that these parts extended over the coating region and are there for a

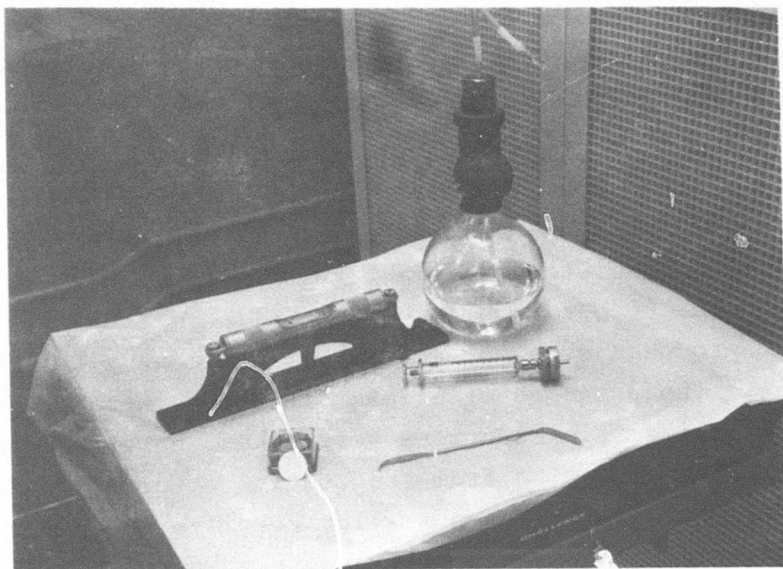


FIGURE 16. COATING TOOLS (The precision level, upper left, a $1.0\ \mu$ nylon filter, lower left. Guth wash bottle, upper right, used for cleaning other instruments. Filter holder (with attached syringe) for TP solution cleaning, middle right. Stir rod, lower right.)

longer period of time during coating does increase the risk of contamination.

After the coating procedure is completed and the coating has set, it is placed in a vacuum bell jar and is heated to about 50°C for at least 24 hours to drive off all remaining solvents.

The solvent used was 48 per cent toluene, 32 per cent methyl ethyl ketone, and 20 per cent ethyl acetate. The thermoplastic was then dissolved in this mix in an amount which measures six per cent by volume. Typically 6.6 cc's of solution was coated onto an area of 600 cm² to produce a solution layer 110 microns thick which upon evaporation produces a thermoplastic layer about 6½ microns thick. The solution was filtered with a 1.0 micron nylon filter, type "NR" produced by Millipore Corp., Bedford, Mass.

An example of coating results is given in Figure 17 which is a composite (10 circular areas) of Mach-Zehnder interferograms of the coated 15" diameter disc. The fringes were intentionally set in during the Mach Zehnder testing. The straightness and parallelism of the fringes indicates very good coating and substrate quality. Thickness uniformity over 2" regions is better than one-fourth wavelength.

The coating method developed for the smaller 5" diameter substrate is similar to that discussed above and has been described in a previous report. Interferograms of the 5" substrate are included here for completeness and are shown in Figure 18. In Figure 18a the interferogram is set for the minimum possible number of fringes which can be seen to be zero. To allow recognition of fractional wavelength nonuniformities not observable in 18a fringes have been included in Figure 18b which is a repeat of 18a except for the Mach-Zehnder fringe pattern setting. Here, better than sixth-wave uniformity has been achieved over a central 1" square region.

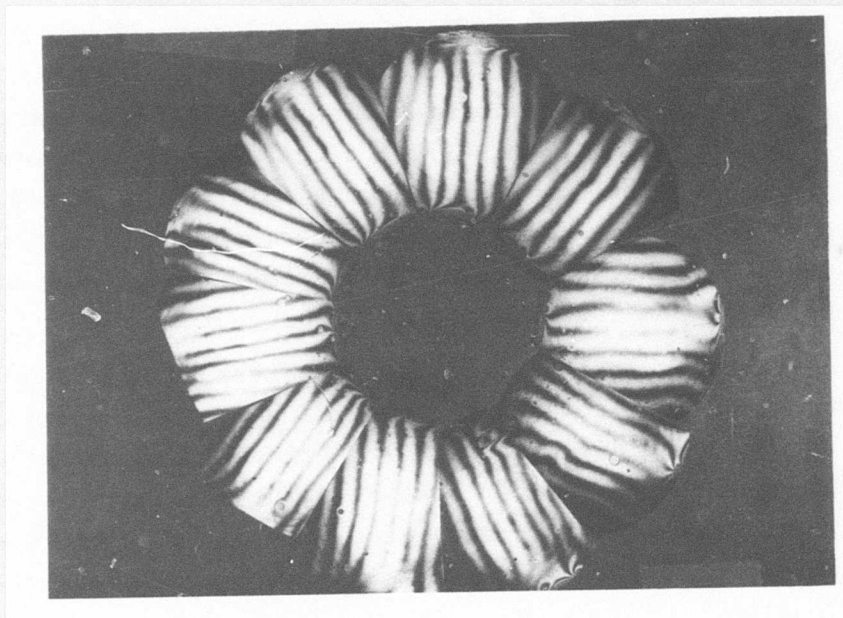
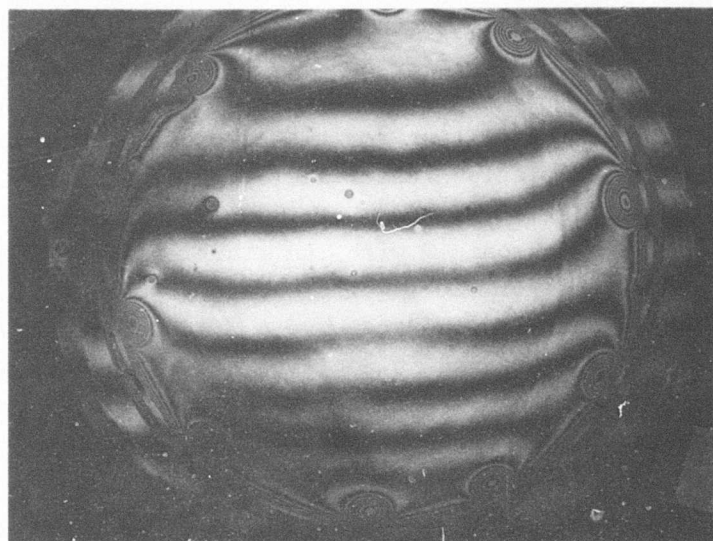
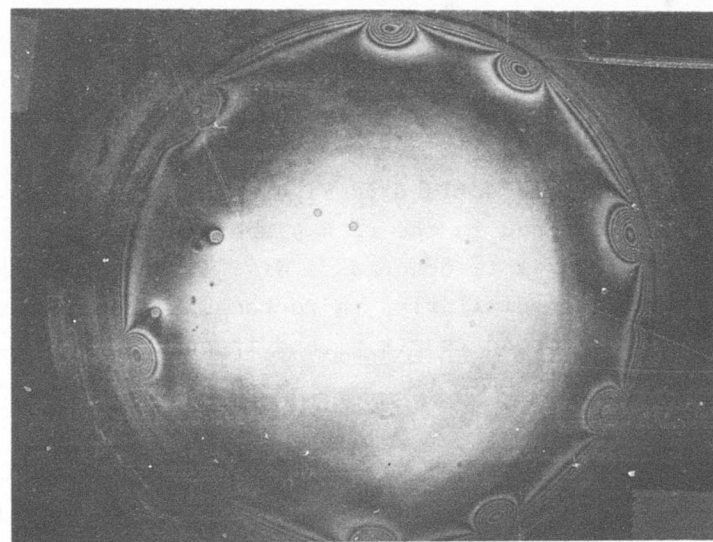


FIGURE 17. COMPOSITE INTERFEROGRAM OF A TP COATED 15" DISC,
(\approx one-fifth size)



(b)



(a)

FIGURE 18. INTERFEROGRAM OF THERMOPLASTIC COATED 5" PLATE.

RECORDING FORMAT

The mathematical formulation for two dimensional Fourier transformations of phase modulation functions (signals) in polar and in rectangular coordinates is reviewed herein. The case of sinusoidal modulation which is synchronized with the start of each scan is treated in Sections 6.1 and 6.2 for rectangular and polar formats. Unsynchronized modulation is analyzed in Section 6.4. Additional analysis of polar format recording is given in Sections 6.3 and 6.5 by methods which allow a more comprehensive treatment of the unusual properties of the Fourier transform of polar data not fully covered in Section 6.2.



FIGURE 19. COORDINATE GEOMETRY

The coordinate geometry is defined in Figure 19. In polar coordinates the input signal is defined in the r, θ plane and is denoted as $g(r, \theta)$. The Fourier transform of g is denoted as $G(\rho, \phi)$ and is defined in the ρ, ϕ (frequency) plane. Similarly, in rectangular coordinates, the input signal to be transformed is $g(x, y)$ and it occurs at the input x, y plane. Its Fourier transform $G(\omega_x, \omega_y)$ is in the frequency plane which has the space variables u, v .

The input data g is assumed to be a light field which is realized by coherent optical readout of recorded data which has been generated as a line scan recording. In the polar format each scan line path occurs in the radial direction and adjacent scan lines are spaced by an angle θ_p with each line having a finite width θ_t . The recorded signal is modulated along each radial scan line. A polar format signal with the modulation $\cos \omega_1 r$ along each scan line is sketched in Figure 20.

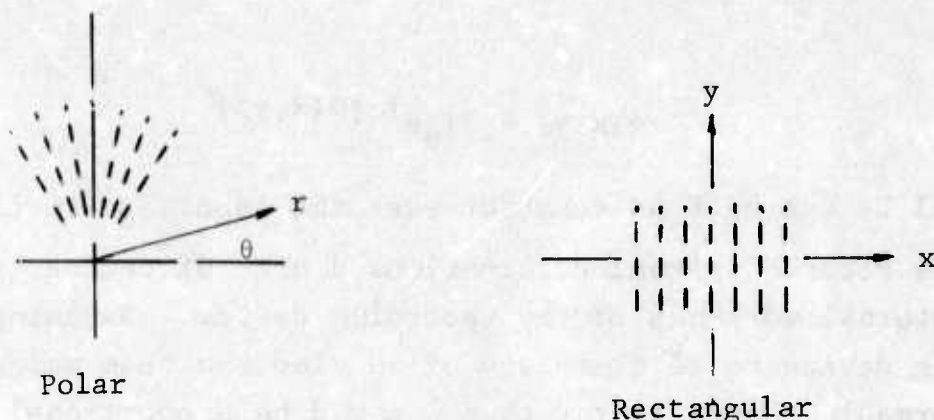


FIGURE 20. INPUT SIGNAL FORMAT

Figure 20 depicts a line scan recording having modulation $\cos \omega_1 y$ along each scan line in the rectangular format. In this case the adjacent scan lines are spaced a distance x_p and each line has a width x_T .

The case of interest here is that of a coherent optical Fourier transform channel where the input data exists in the form of variations in the complex optical transmission $t = Te^{j\alpha}$ of the recording medium. In particular, the recorded data will be in the form of a surface deformation modulation denoted by deformation depth d . The deformation modulation will affect the phase α of the optical transmission function t . The transmissivity T is constant ($T = T_0$). Upon readout with a collimated coherent light beam which illuminates the area of the input data to be processed we realize for our input signal a light beam emergent from the recording medium which is equal to the product of the illumination light field amplitude E and the complex optical transmission t . Thus, the input g , can be expressed generally, in polar form, as

$$g(r, \theta) = ET_0 e^{j\alpha[d(r, \theta)]}$$

and in rectangular form as

$$g(x,y) = ET_0 e^{j\alpha[d(x,y)]}$$

We will be taking E as constant over the input aperture.

The recorded signal deformations d are, of course, related to the internal workings of the recording device. Assuming the recording device to be comprised of an electron beam which writes on a deformable thermoplastic then d would be proportional to the recorder input that is used to modulate the writing electron beam. The performance of the recording device will not be considered explicitly here.

At the output, or frequency plane, we obtain the optical Fourier transform G of the input g , i.e., $G = F[g]$. The transform in polar coordinates for polar format input data can be expressed as

$$G(\rho, \phi) = A \int dr \cdot r \int d\theta \cdot g(r, \theta) e^{-j2\pi r \cos(\theta - \phi)}$$

It should be noted that this expression represents a Fourier transform in the ρ dimension only because it is based upon optical processing elements having circular symmetry such that no optical power occurs in the circular dimension.

In rectangular coordinates we have the Fourier transform expression

$$\bar{G}(\omega_x, \omega_y) = A \iint g(x,y) e^{-j(\omega_x x + \omega_y y)} dx dy$$

This rectangular coordinate expression is also based on optical processing elements having circular symmetry as with a spherical lens for example.

The term A appearing before the transform integral contains the amplitude constants and the phase terms of the coherent optical Fourier transformation process which are not dependent on the variables of integration.

6.1 RECTANGULAR FORMAT DATA

The input $g(x,y)$ to be transformed is the rectangular format line scan phase recording with sinusoidal modulation in the scan line direction y , as sketched in Figure 20. The scan line deformation grooves in the y direction are periodic in the variable x with period x_p and width x_T . The x direction deformation variation is described by a function $h(x)$ that is normalized relative to the peak deformation D_x and can be expressed generally as a Fourier series

$$h(x) = \sum_k C_k \cos \frac{2\pi k}{x_p} x$$

where

$$C_k = \frac{1}{x_T} \int_{-x_T/2}^{x_T/2} h(x) \cos \left(\frac{2\pi k}{x_p} x \right) dx$$

A sinusoidal modulation in y along each scan line is denoted as

$$f(y) = D \cos \omega_1 y$$

The two dimensional deformation expression is then

$$d(x,y) = (D_x + D \cos \omega_1 y) \sum_k C_k \cos k\omega_0 x$$

where ω_0 is the scan line spacing frequency, i.e., $\omega_0 = \frac{2\pi}{x_p}$. The input signal to be transformed is now

$$\begin{aligned} g(x,y) &= ET_0 e^{j \frac{2\pi(n-1)}{\lambda}} (D_x + D \cos \omega_1 y) \sum_k C_k \cos k\omega_0 x \\ &= ET_0 e^{j \left[a \sum_k C_k \cos k\omega_0 x + b \sum_k C_k \cos(k\omega_0 x \pm \omega_1 y) \right]} \end{aligned}$$

where

$$a = \frac{2\pi(n-1)}{\lambda} D_x$$

$$b = \frac{2\pi(n-1)}{\lambda} D/2$$

The Fourier transform $G(\omega_x, \omega_y)$ is now written as

$$\begin{aligned}
G(\omega_x, \omega_y) &= B \int_{-y_1/2}^{y_1/2} \int_{-x_1/2}^{x_1/2} e^{j \left[a \sum_k C_k \cos k \omega_0 x + b \sum_k C_k \cos (k \omega_0 x \pm \omega_1 y) \right]} \\
&\quad \cdot e^{-j(\omega_x x + \omega_y y)} dx dy \\
&= B \int_{-y_1/2}^{y_1/2} \int_{-x_1/2}^{x_1/2} \prod_k \left[\sum_{\ell, m} (-j)^{\ell+m} J_\ell(a C_k) e^{j \ell k \omega_0 x} J_m(b C_k) e^{j m (k \omega_0 x \pm \omega_1 y)} \right] \\
&\quad \cdot e^{-j(\omega_x x + \omega_y y)} dx dy
\end{aligned}$$

If we take the scan line cross-section $h(x)$ to be simply a sinusoid $C \cos \omega_0 x$ rather than a general series $\sum C_k \cos k \omega_0 x$, as is very nearly the case, we get

$$\begin{aligned}
G(\omega_x, \omega_y) &= B \sum_{\ell, m} J_\ell(a C) J_m(b C) \frac{x_1}{2} \frac{\sin \frac{1}{2} (\omega_x + (\ell+m) \omega_0)}{\frac{x_1}{2} (\omega_x + (\ell+m) \omega_0)} \\
&\quad \cdot \frac{y_1}{2} \frac{\sin \frac{1}{2} (\omega_y \pm m \omega_1)}{\frac{y_1}{2} (\omega_y \pm m \omega_1)}
\end{aligned}$$

Here we have used a rectangular input data aperture over $-x_1/2 \leq x \leq x_1/2$ and $-y_1/2 \leq y \leq y_1/2$ and have collected non-integrand terms in B.

The light intensity distribution $|G(\omega_x, \omega_y)|^2$ which is available for observation in the transform plane is expressed as

$$|G(\omega_x, \omega_y)|^2 = |B|^2 \frac{x_1 y_1}{4}^2 \sum_{\ell, m} J_{\ell}^2(aC_1) J_m^2(bC_1) \text{Sinc}^2(\omega_x + (\ell+m)\omega_0) \\ \cdot \frac{x_1}{2} \text{Sinc}^2(\omega_y + m\omega_1) \frac{y_1}{2}$$

for cases where there is insignificant overlap of orders. Thus we get spots of light in the frequency plane located at (ω_x, ω_y) with $\omega_x = (\ell+m)\omega_0$ and $\omega_y = m\omega_1$. The peak intensity is proportional to recorded deformation depth through the arguments a and b in $J_{\ell}^2[]$ and $J_m^2[]$. The spatial distribution of the light spots is given by the Sinc function. In practical use for spectrum analysis of the recorded data we choose recorded depths to retain mainly two pairs of spots of light in the frequency plane ($\omega_y = \pm\omega_1, \omega_x = \omega_0$) for any one recorded input frequency ω_1 .

6.2 POLAR FORMAT DATA

The input $g(r, \theta)$ to be transformed will be the polar format line scan recording with sinusoidal modulation in the line direction as sketched in Figure 20. The scan lines are straight deformation grooves in the r direction which will be periodic in the polar angle variable θ with period θ_p , groove width θ_t and mean groove depth D_{θ} . The angles θ , θ_p , and θ_t are in radians and D_{θ} in millimeters. The scan line is of constant width in linear measure. Its angular width θ_t will vary inversely with r . The scan line description in the θ direction will be denoted by a function h which is normalized relative to the peak depth D_{θ} . Since it is periodic in θ we can express h with the following Fourier series

$$h(r, \theta) = \sum_k C_k(r) \cos \frac{2\pi k}{\theta_p} \theta$$

where

$$C_k = \frac{1}{\theta_T} \int_{-\frac{\theta_T}{2}}^{\frac{\theta_T}{2}} h(\theta) \cos \frac{2\pi k}{\theta_p} \theta d\theta$$

Deformation modulation along the scan line, denoted as the function f will be sinusoidal with peak deformation D and frequency ω_1 , thus,

$$f(r) = D \cos \omega_1 r$$

The composite recording in r and θ is written as

$$d(r, \theta) = (D_\theta + D \cos \omega_1 r) \sum_k C_k(r) \cos k\omega_\theta \theta$$

where ω_θ is the scan line spacing frequency, i.e., $\omega_\theta = \frac{2\pi}{\theta_p}$. The signal to be transformed $g(r, \theta)$ is expressed as

$$\begin{aligned} g(r, \theta) &= ET_o e^{j \frac{2\pi(n-1)}{\lambda} (D_\theta + D \cos \omega_1 r) \sum_k C_k(r) \cos k\omega_\theta \theta} \\ &= ET_o e^{j \left[a \sum_k C_k(r) \cos k\omega_\theta \theta + b \sum_k C_k(r) \cos(k\omega_\theta \theta \pm \omega_1 r) \right]} \end{aligned}$$

where $a = \frac{2\pi(n-1)}{\lambda} D_\theta$ and $b = \frac{2\pi(n-1)}{\lambda} D/2$.

Using the Bessel series expansion for the exponential terms in $g(r, \theta)$, its transform can be expressed as

$$G(\rho, \phi) = B \int dr r \int d\theta \cdot \prod_k \sum_{\ell, m, n} (-j)^{\ell+m+n} J_\ell(aC_k) J_m(bC_k) J_n(cr) e^{j\ell k \omega_\theta \theta}$$

$$e^{jm(k\omega_\theta \theta \pm r)} e^{-jn(\theta - \phi)}$$

where $B = AET_{\theta_0}$, $c = 2\pi\rho = \omega_\theta$ and the limits of integration for θ are $\theta_0 - \frac{1}{2}$ to $\theta + \frac{1}{2}$ and for r are $r_0 - \frac{r_1}{2}$ to $r_0 + \frac{r_1}{2}$.

We will continue with the assumption that the scan line cross section is sinusoidal in θ giving $C \cos \omega_\theta \theta$ rather than $C_k \cos k\omega_\theta \theta$. The integration on θ is then as follows.

$$\int_{-\frac{\theta_1}{2}}^{\frac{\theta_1}{2}} e^{j[(\ell+m)\omega_\theta - n]\theta} d\theta e^{jn\phi}$$

$$= \frac{\theta_1}{2} e^{-j(\ell+m)\omega_\theta} e^{jq\phi} \left[\frac{\sin q \frac{\theta_1}{2}}{q \frac{\theta_1}{2}} \right]$$

where $q = (\ell+m)\omega_\theta - n$

We must note here that $\omega_\theta = 2\pi \frac{1}{\theta_p}$ where $\theta_p = \frac{2\pi}{N}$ and N is very large ($<10^4$). The above result contains a Fourier series expansion over q which defines a pulse of width θ_1 in the ϕ dimension of the frequency plane. The pulse has period 2π and can have fine structure within the pulse depending upon the Sinc function be-

havior over the index variable q . The pulse in ϕ has width θ_1 which is identical to the input plane pulse width θ . The polar format Fourier transformation now has the form

$$G(\rho, \phi) = \frac{B\theta_1}{2} \int_{r_0 - \frac{r_1}{2}}^{r_0 + \frac{r_1}{2}} dr \cdot r \cdot \sum_{\ell, m, n} (-j)^{\ell+m+n} J_{\ell}(aC_{\ell}) J_m(bC_{\ell}) J_n(cr) \cdot e^{jm\omega_1 r - jn\phi} \frac{\sin q \frac{\theta_1}{2}}{q \frac{\theta_1}{2}}$$

We will continue with the integration on r with the approximations that $\text{Sinc}(q)$ is separable from the series on J_n and that the integrand term r has a minor effect and is taken constant over the range of the integration. With these assumptions, we can write G as

$$G(\rho, \phi) = \frac{B\theta_1}{2} \sum_{\ell, m, q} (-j)^{\ell+m} J_{\ell}(aC) J_m(bC) e^{-jn\phi} \frac{\sin q \frac{\theta_1}{2}}{q \frac{\theta_1}{2}} \cdot \int_{r_0 - \frac{r_1}{2}}^{r_0 + \frac{r_1}{2}} dr \sum_n (-j)^n J_n(cr) e^{\pm jm\omega_1 r}$$

The assumption that $\text{Sinc}(q)$ is separable from the J_n series appears reasonable because the value of ω_{θ} is very large. With the separability

assumption the J_n series exists alone under the integral operator and can be changed as follows:

$$\sum (-j)^n J_n(cr) = e^{jcr}, \text{ where } c = 2\pi\rho = \omega_\rho$$

The integral on r has the form

$$\int_{r_0 - \frac{r_1}{2}}^{r_0 + \frac{r_1}{2}} e^{j(c \pm m\omega_1)r} dr = \frac{r_1}{2} \frac{\sin(\omega_\rho \pm m\omega_1) \frac{r_1}{2}}{(\omega_\rho \pm m\omega_1) \frac{r_1}{2}} e^{j(\omega_\rho \pm m\omega_1)r_0}$$

This approximation for the Fourier transform $G(\rho, \phi)$ is thus

$$\begin{aligned} G(\rho, \phi) &= \frac{B\theta_1 r_1}{4} \sum_{\ell, m, n} (-j)^{\ell+m} J_\ell(aC) J_m(bC) \frac{\sin q \frac{\theta_1}{2}}{q \frac{\theta_1}{2}} e^{-jn\phi} \\ &\quad \cdot \frac{\sin(\omega_\rho \pm m\omega_1) \frac{r_1}{2}}{(\omega_\rho \pm m\omega_1) \frac{r_1}{2}} e^{j(\omega_\rho \pm m\omega_1)r_0} \\ &= \frac{B\theta_1 r_1}{4} \sum_m \tilde{g}(\phi) \text{Rect}(\phi/\theta_1) \frac{\sin(\omega_\rho \pm m\omega_1) \frac{r_1}{2}}{(\omega_\rho \pm m\omega_1) \frac{r_1}{2}} e^{j(\omega_\rho \pm m\omega_1)r_0} \end{aligned}$$

We note that the combined terms $J_\ell J_m e^{j[(1+m)\omega_\rho - q]\phi} \sin q \frac{\theta_1}{2} \div \frac{\theta_1}{2} q$ are a Fourier series for the original $g(\theta) \cdot \frac{1}{ET_0}$ (with $\cos \omega_1 r = 1$) but now in the variable ϕ , i.e., $\tilde{g}(\phi)$ taken over the interval $-\frac{\theta_1}{2} \leq \phi \leq \frac{\theta_1}{2}$ as indicated by the $\text{rect}(\phi/\theta_1)$ function.

The light intensity distribution $|G(\rho, \phi)|^2$ is available for observation in the transform plane and it is expressed as

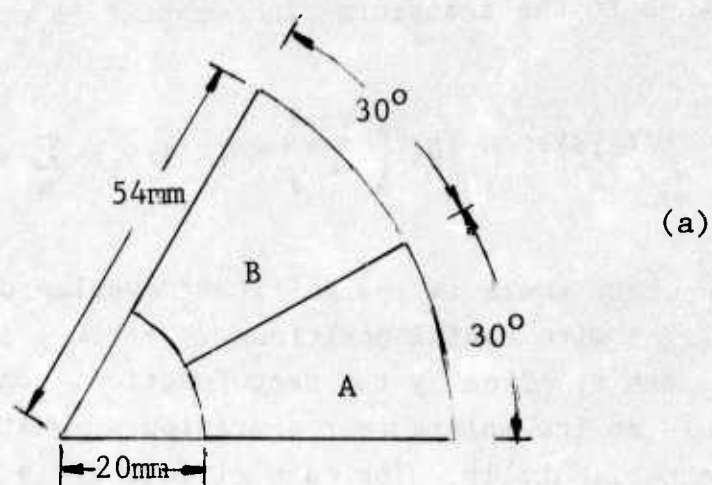
$$|G(\rho, \phi)|^2 = |B|^2 \left(\frac{\theta_1 r_1}{4} \right)^2 \text{Rect}(\phi/\theta_1) \sum_m \text{sinc}^2 \left[(\omega_\rho \pm m\omega_1) \frac{r_1}{2\pi} \right]$$

for cases where there is insignificant overlap of orders. We get arcs of light with radial positions $\omega_\rho = \pm m\omega_1$ and the arcs have angular width θ_1 given by the rect function. This approximate solution is an incomplete representation of what can be demonstrated experimentally. The main difference is the absence of terms representing higher order diffraction in the ϕ direction. An alternative approach to the analysis of polar format data is given in Sections 6.3 and 6.5.

6.3 EXPERIMENTAL ANALYSIS OF POLAR DATA

It is important to review experimental results for the optical Fourier transform of polar formatted data as a guide when deriving a mathematical representation of frequency plane distributions. Experimental analysis of data recorded in a polar format was accomplished with inputs of the form shown in Figure 21 which consists of two adjacent 30° sectors each with synchronized pulse modulation. The ratio of the pulse repetition rate of sections A to B is 5 to 3. Other specifics are given in the figure.

The first few transforms to be considered are apertured sections of the transparency. The aperture was a 7.5° angular sector as illustrated in Figure 21b. When placed over section A, the transform shown in Figure 22 was obtained, and when over B, the transform shown in Figure 23 was obtained. The vertical direction f_y corresponds to the centerline direction y of the input aperture (see Figure 21b). A study of these transforms



Radial (r) Mod: A: 3.1 c/mm
Pulsed (50% duty) B: 1.8 c/mm

Circ (θ) Mod: 4.1 λ /deg
Pulse (Scan Lines)

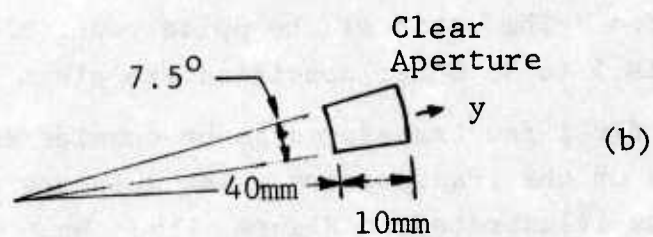


FIGURE 21. POLAR RECORDING

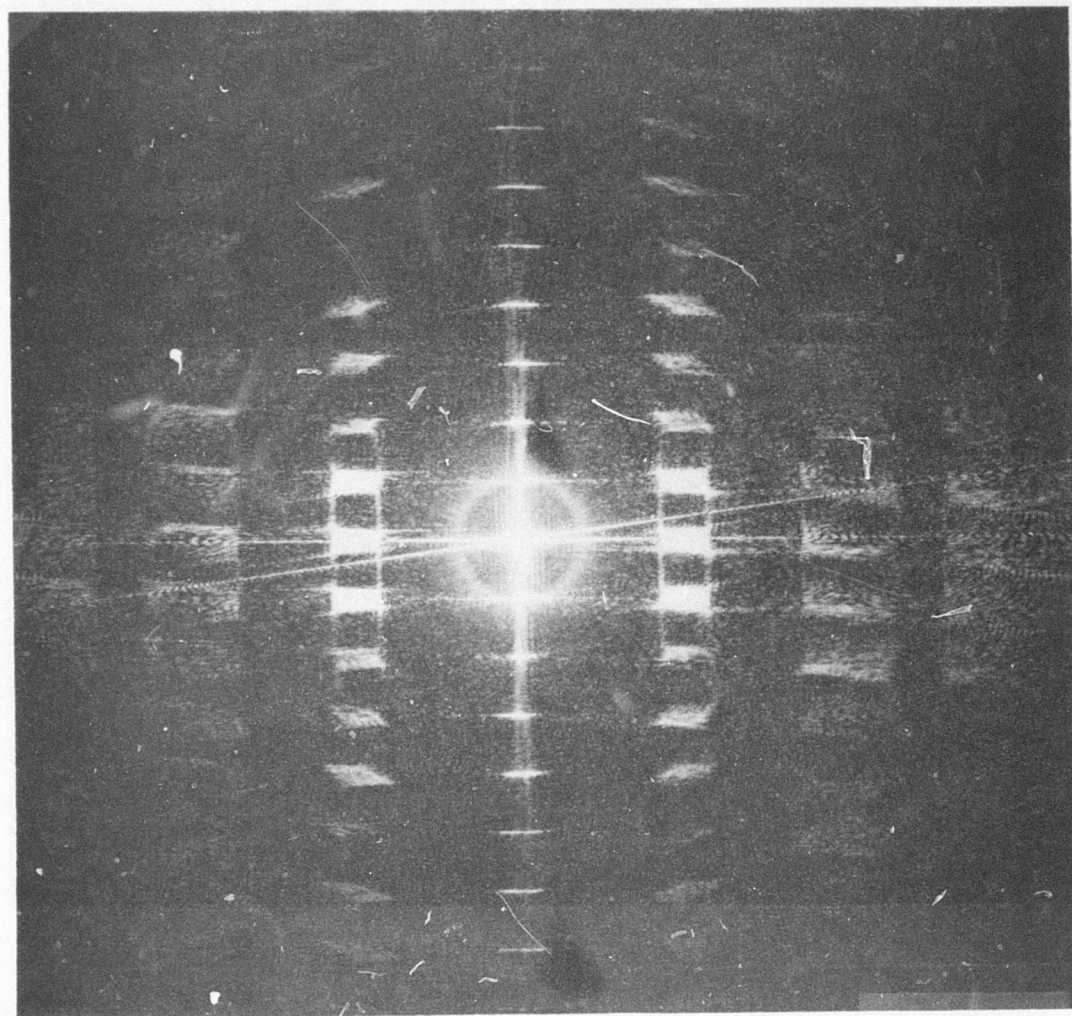


FIGURE 22. FREQUENCY PLANE FOR INPUT APERTURE A

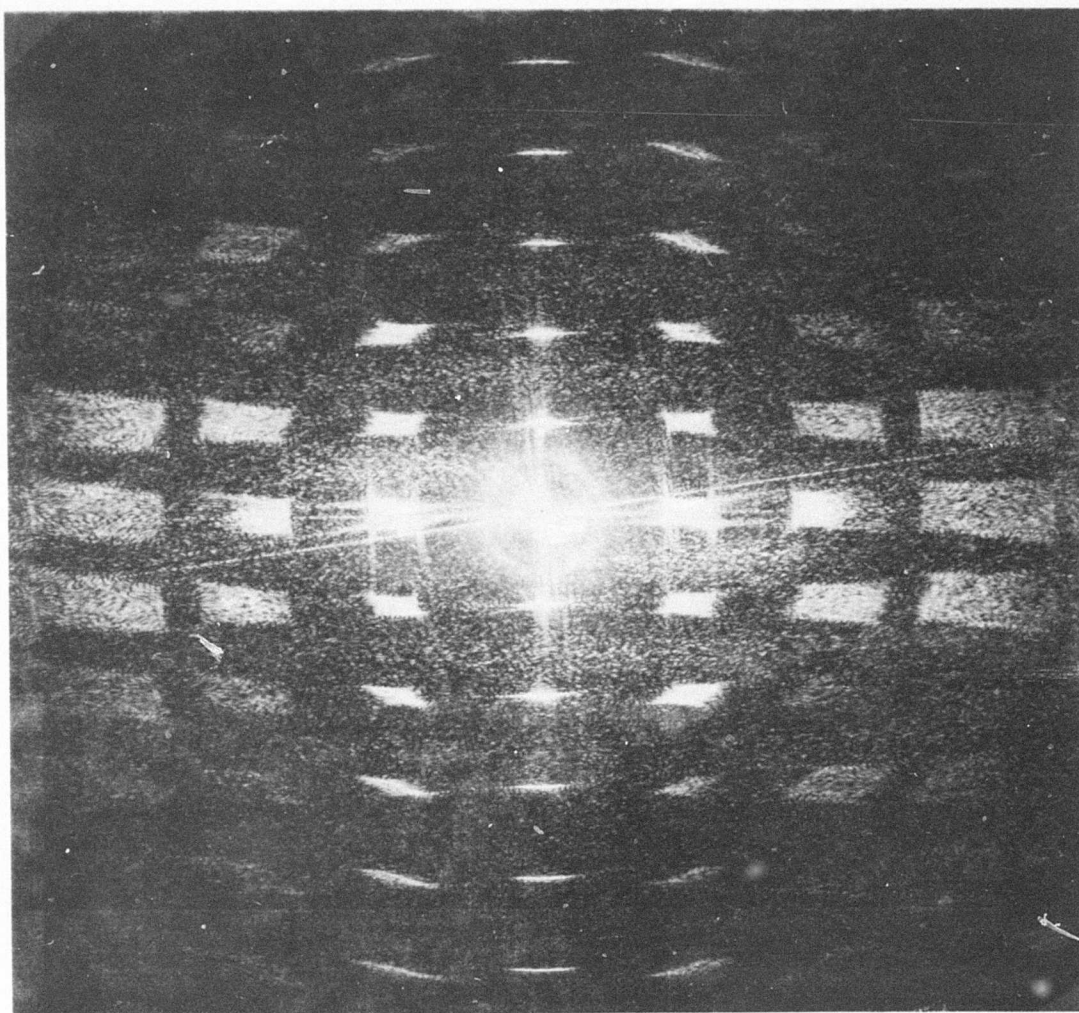


FIGURE 23. FREQUENCY PLANE FOR INPUT APERTURE B

indicates that pulse modulation in the input plane produces characteristics in the transform plane that are discussed below and shown graphically in Figure 24

1. A multiplicity of orders for which each "center of mass" is on a rectangular grid with coordinates

$$(f_x, f_y) = \left(\frac{M}{\theta_p R_{\text{mean}}}, \frac{N}{R_p} \right)$$

where

M & N are the order number as indicated in Figure 24

$R_{\text{mean}} = \frac{R_b + R_a}{2}$ is the mean position of the aperture,

R_p is the pulse modulation period,

θ_p is the azimuthal period of the scan lines

Each order is confined to an area about its center of mass, where the area is distorted with respect to the input aperture and where the distortion depends on the order number.

2. The orders along the f_y direction are contained in angle θ_A about f_y , where θ_A is the input aperture angle. These orders are the FT of the pulse modulation, e.g. the orders occur for $f_y = \frac{\text{integer}}{R_p}$, and their width along f_y is inversely proportional to the scan line length $R_b - R_a$.
3. The orthogonal direction f_x represents the frequency content or shape of the scan lines. If we define a tangential frequency $\omega = \frac{1}{\theta_p R}$ in the input plane (i.e. the spatial frequency of the scan lines along a circle of radius R) then the Mth order (along f_x where $N = 0$) is confined to the interval $\frac{M}{\theta_p R_b}$ to $\frac{M}{\theta_p R_a}$. That is, it is confined to

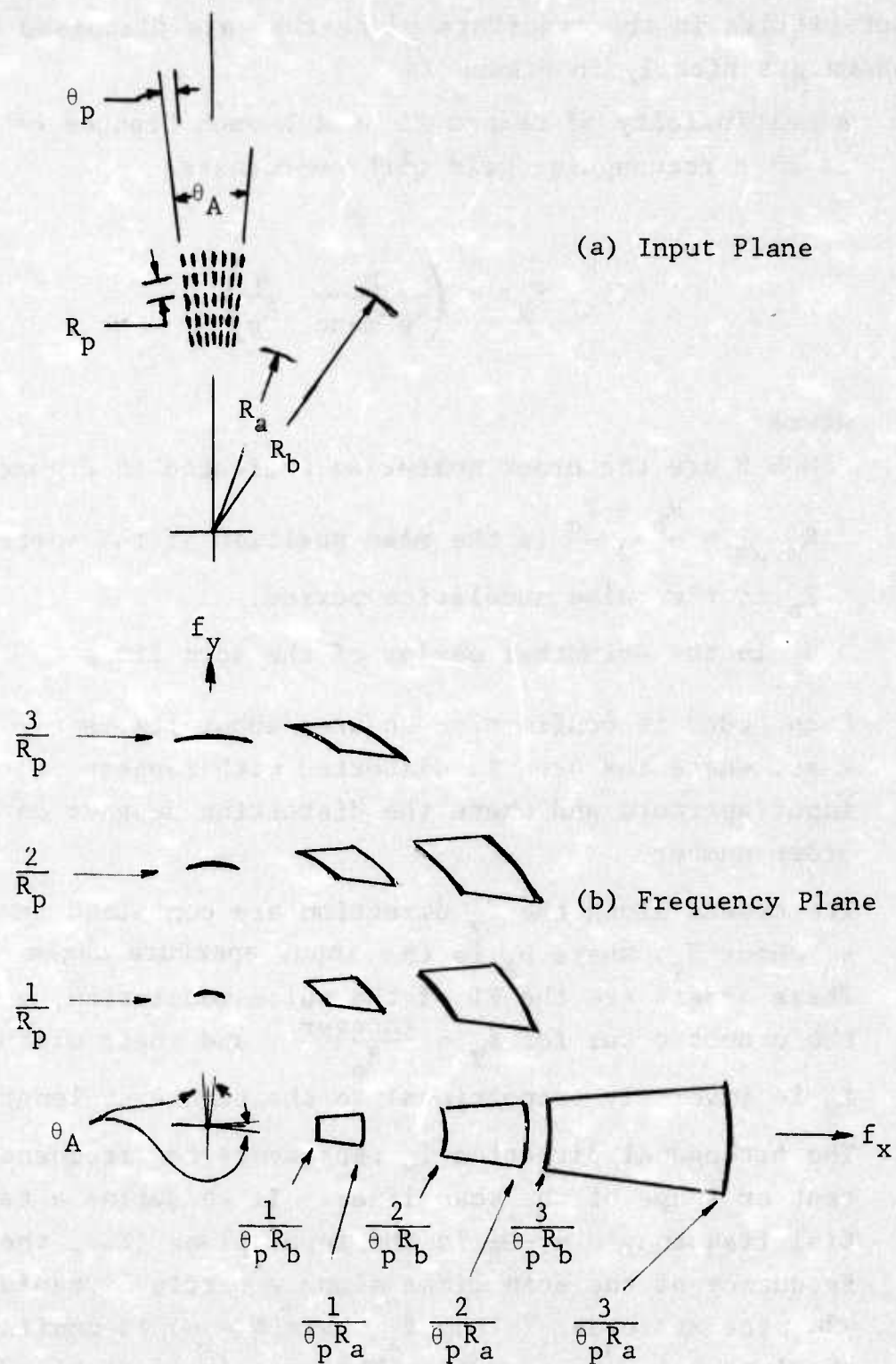


FIGURE 24. FREQUENCY PLANE POLAR PARAMETERS

the extremum tangential frequencies of the input and there is an inverse relationship of the nature that if the aperture is closed down from the outside (i.e. R_b reduced) then the orders along f_x reduce in size from the inside. This means that the orders along f_x will eventually overlap since their size increases with the order.

We also note that these orthogonal orders are contained within the aperture angle θ_A centered along f_x axis

4. There does not seem to be any well defined fringe structure within any order except when orders overlap. This latter result is seen in Figure 25 for which the aperture of Figure 21b was centered on the boundary between both sections, i.e., 3.25° of section A and 3.25° of section B. Regions of overlap between the two sets of orders for the two different sections produce fringes indicative of the pulse modulation ratios of the two sections. Figure 26 is for the same kind of setup as for Figure 25 but where the radius R_a of the aperture was reduced to 2 mm. This figure shows both the interference effects between the different orders and the inverse characteristic of the orthogonal orders described in (3) above. The flaring seen at the end of the orders is due to the smearing together of the scan line and pulse modulation at the smaller radii on the transparency.

Finally the transform for the entire transparency (60° sector) is shown in Figure 27. There is significant overlap of many orders. If the FT orders along the f_y -direction, within the θ_T angle, are to be clear of any other orders then from geometrical consideration in Figure 24 we need to specify that

$$f_{\max} \tan \theta_A > \frac{1}{\theta_p R_b}$$

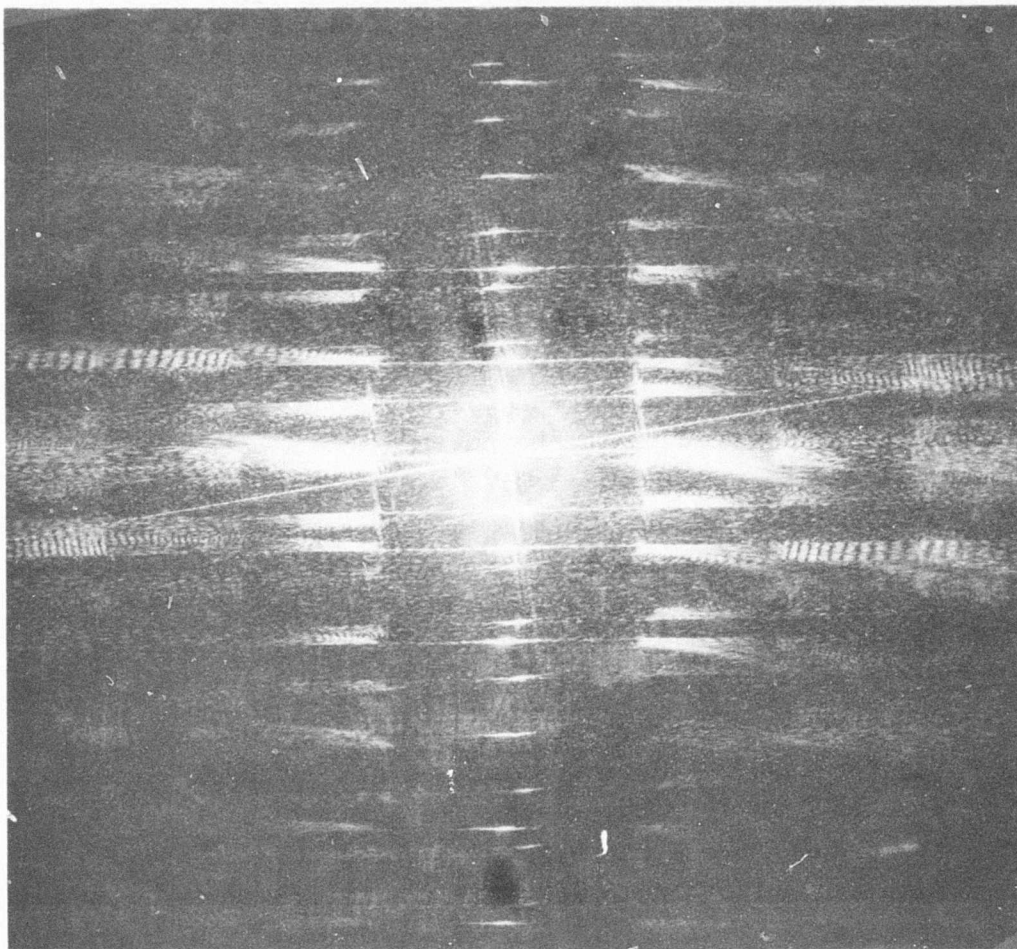


FIGURE 25. FREQUENCY PLANE - TWO INPUT SIGNALS ,
SMALL APERTURE

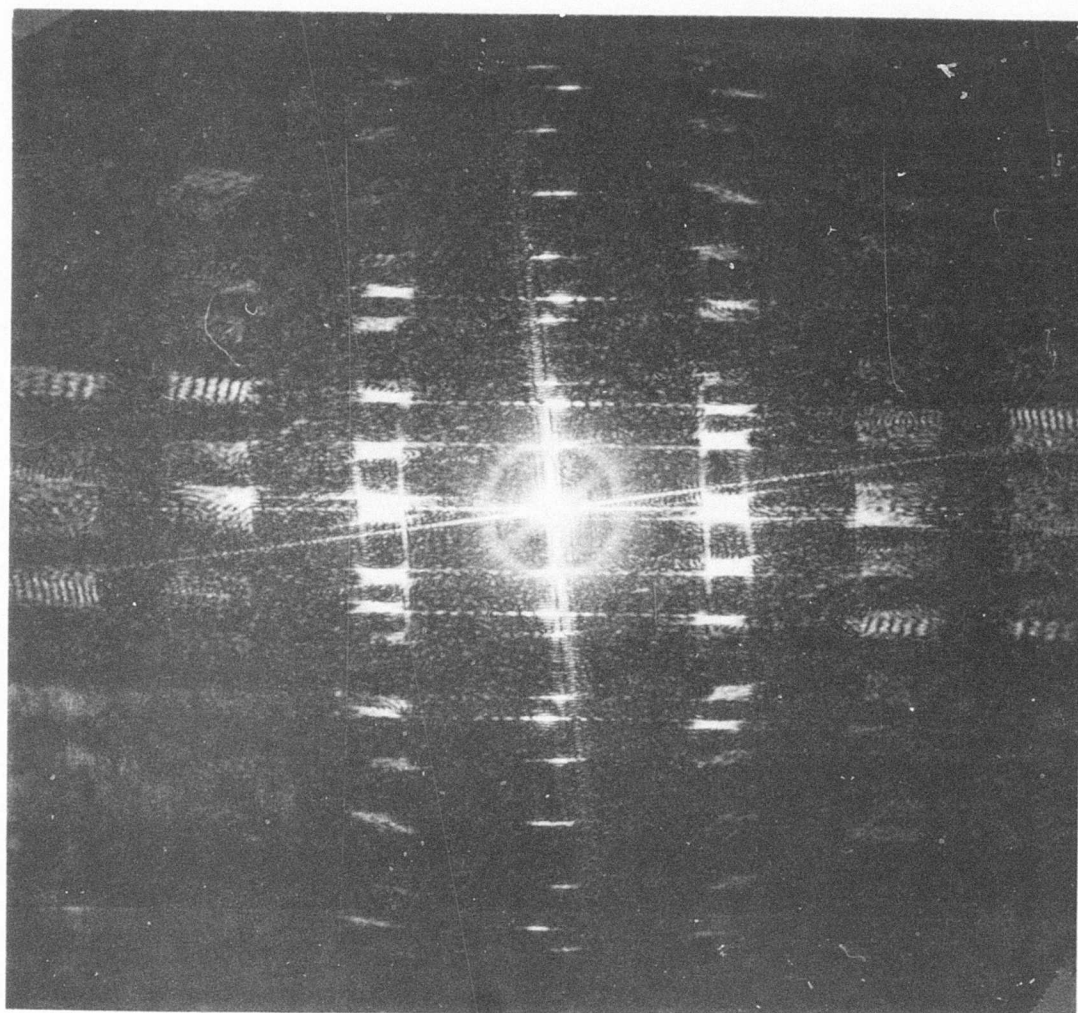


FIGURE 26. FREQUENCY PLANE - TWO INPUT SIGNALS,
INCREASED RADIAL APERTURE

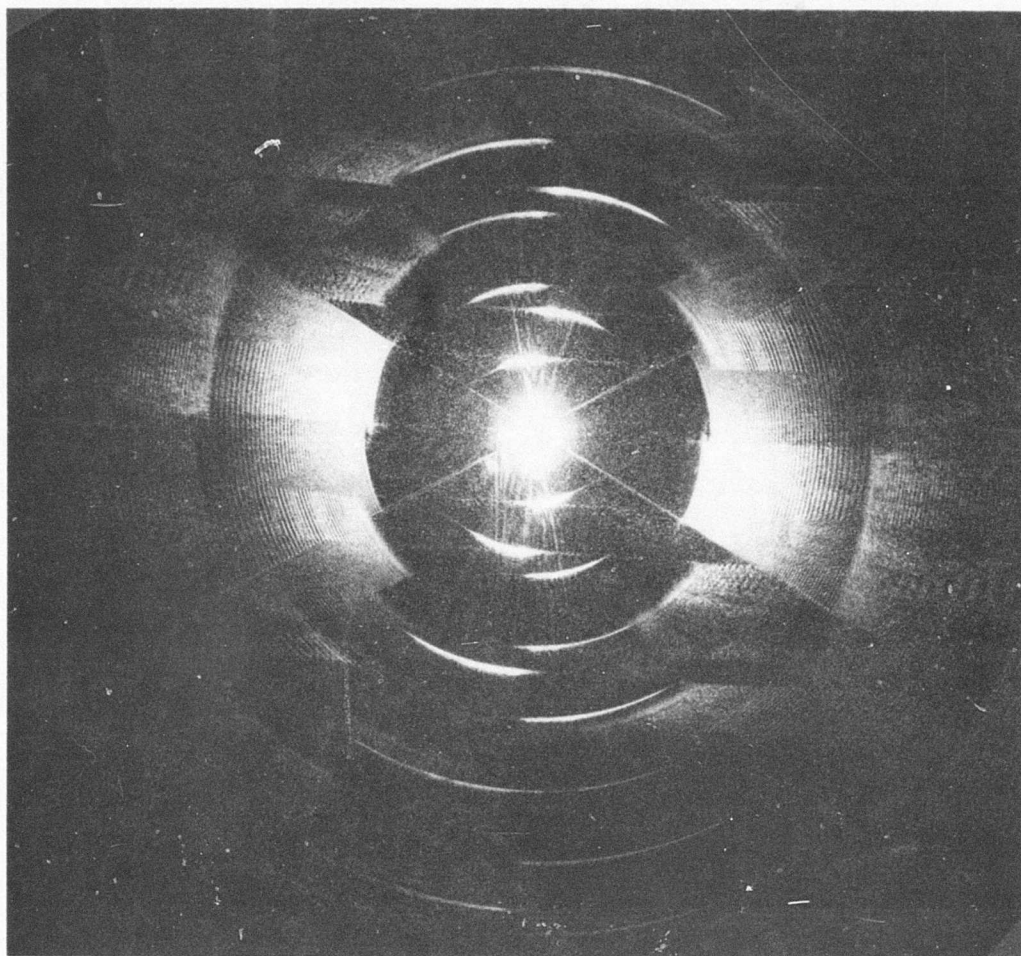


FIGURE 27. TWO INPUT SIGNALS, LARGE APERTURE

or

$$\theta_A > \arctan(\theta_p R_b f_{\max})^{-1}$$

where f_{\max} is the maximum spatial frequency of interest.

An alternative to the above criteria may be to eliminate the higher order $M, N > 1$ by using a scan line with a sinusoidal cross section that linearly expands with R such that there is only a single azimuthal frequency. It has not been shown experimentally that such a condition does indeed eliminate the higher orders.

It should be pointed out that many of the observations made are dependent on the input aperture being not too small (in order to avoid significant aperture diffraction effects) and not too large (in order to avoid overlapping orders).

6.4 UNSYNCHRONIZED MODULATION COUPLING

The example of sinusoidal phase modulation along scan lines, in either polar or rectangular format, was described in the previous sections in a way which assumed that the phase of the sinusoid was the same at the start of each scan, i.e., synchronized. When this condition is not satisfied then frequencies can be generated in the direction orthogonal to the scan lines.

In the rectangular format, if we consider some arbitrary modulation frequency f_1 in the scan line direction and a scan line repetition frequency f_s , then it can be shown that we can realize synchronized recording if f_1 is an integer multiple of f_s . That is, if q is an integer, we require for synchronization that

$$f_1 = qf_s$$

when the above relationship does not hold true and f_1 is some value between $(q + 1)f_s$ and qf_s we can define the value of frequency induced in the direction orthogonal to the scan line as follows. First we examine f_1 relative to f_s and determine numbers n and a such that

$$f_1 = (n + a) f_s = nf_s + af_s$$

with the constraints that n = positive integer, $1 < a \leq 0$.

Then the resultant spatial frequency component f_a in the direction orthogonal to the scan lines (x direction for the rectangular format) is

$$f_a = \frac{af_s y_p}{x_p}$$

Here f_1 , f_a and f_s are spatial frequencies, y_p is the spatial equivalent of the temporal scan period and x_p is the spatial spacing between successive scan lines.

A similar result exists for the polar format except that we work in the variables r and θ . Thus, in the polar format we have

$$f_a = \frac{af_s R_p}{\theta_p}$$

We must introduce this added modulation to the input signal functions for the respective cases of $g(x,y)$ and $g(r,\theta)$. It must be included as a phase function which is added to the sinusoid of frequency f_1 which was considered in the above discussion.

Thus in rectangular coordinates, the scan line modulation $D \cos \omega_1 y$ goes to $D \cos (\omega_1 y + \omega_a x)$. In polar coordinates $D \cos \omega_1 r$ goes to $D \cos (\omega_1 r + \omega_a \theta)$.

Regarding resolution in the frequency plane we note (in the rectangular format variables) that a spot of light in the frequency plane will be located along loci which are a set of parallel sloped lines in the ω_y, ω_x plane. This can be seen by examining the Fourier transform expression $G(\omega_x, \omega_y)$ when the ω_a term is included. The slope of the loci in the ω_y, ω_x plane is

$$\frac{x_p}{y_p} = \text{slope of loci}$$

The set of loci cross the ω_y axis at the frequency

$$\omega_y = q\omega_s, \text{ loci crossing on } \omega_y \text{ axis}$$

The line spacing of the loci in the ω_y and ω_x directions are

$$\omega_s = \text{loci spacing in } \omega_y \text{ direction}$$

$$\omega_s \frac{y_p}{x_p} = \text{loci spacing in } \omega_x \text{ direction}$$

The width of a single frequency spot in ω_y and ω_x is defined by the sinc function expressions of the Fourier transform $G(\omega_x, \omega_y)$

where we find the spot half width from its center to its first zero is

$$\Delta\omega_y = \frac{2\pi}{y_1}, \text{ for } \omega_y \text{ direction}$$

and

$$\Delta\omega_x = \frac{2\pi}{x_1}, \text{ for } \omega_x \text{ direction}$$

And, for comparison the ratio of spot width to loci separation in the two dimensions is seen to be

$$\frac{2\pi}{\omega_s y_1} = 1, \text{ for } \omega_y \text{ direction}$$

$$\frac{2\pi x_p}{\omega_s y_p x_1} = \frac{x_T}{x_1}, \text{ for } \omega_x \text{ direction}$$

Improved resolutions in the ω_y direction is desirable and may be available by use of double raster recordings .

6.5 FURTHER DERIVATION OF POLAR DATA TRANSFORM

In this section an expression for the Fourier Transform (FT) of polar formatted data will be discussed which describes higher order diffraction in both the dimensions of the frequency plane ρ , ϕ rather than only one dimension as described in Section 6.2. This analysis assumes recorded data which can be represented as optical transmission variations. This will be true for phase modulation where recorded deformation depths are small.

First we will consider a series of polar scan lines with no modulation along the scan line in order to determine the FT of the basic system. A single scan line of length $R_b - R_a = \Delta R$ and constant width W is described by (see Fig 28a)

$$\text{rect}\left(\frac{x}{W}\right)\text{rect}\left(\frac{y}{\Delta R}\right)*\delta(y - \Delta R_c)$$

where $R_c = \frac{R_a + R_b}{2}$. Then its FT is $W\Delta R \text{sinc}(Wf_x)\text{sinc}(\Delta Rf_y)e^{-2\pi if_y R_c}$. The transform in polar coordinates (ρ, ϕ) is

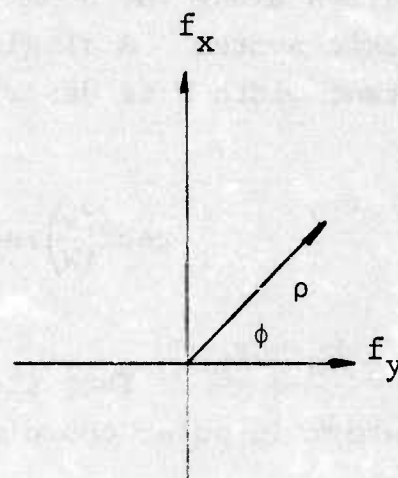
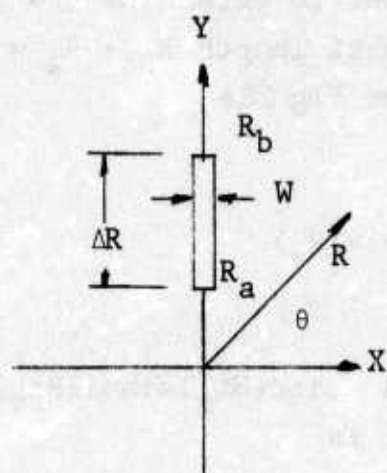
$$W\Delta R \text{sinc}(W\rho\cos\phi)\text{sinc}(\Delta R\rho\sin\phi)e^{-2\pi i R_c \rho\sin\phi}$$

If there are N scan lines, separated by the azimuth period θ_p , then the total signal is (see Fig 28b)

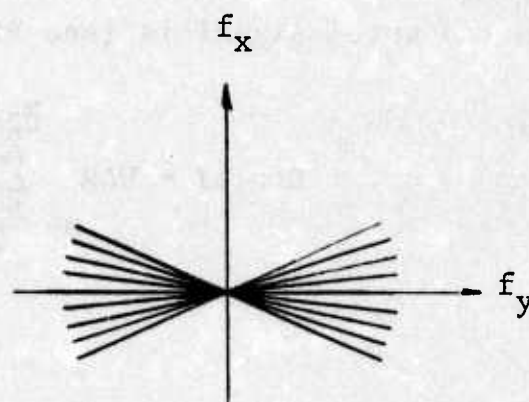
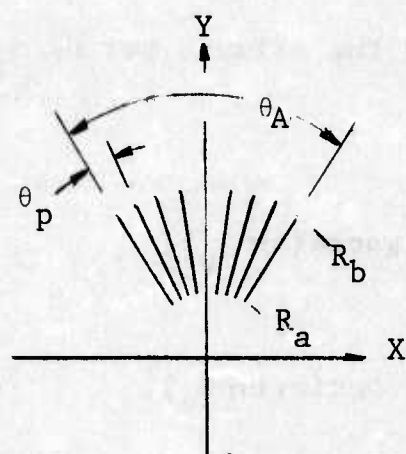
$$G(\rho, \phi) = W\Delta R \sum_{n=-\frac{N-1}{2}}^{\frac{N-1}{2}} \text{sinc}[W\rho\cos(\phi+n\theta_p)] \cdot \text{sinc}[\Delta R\rho\sin(\phi+n\theta_p)] \cdot e^{-2\pi i R_c \rho\sin(\phi+n\theta_p)} \quad (1)$$

where for convenience we let N be an odd integer. This equation (1) is our basic relationship. Let us now consider the conditions under which this expression is to apply. First we have that (see Fig. 28b)

$$\theta_A = N\theta_p < \frac{\pi}{4} \quad (2a)$$



(a)



$$P = \frac{2\pi}{\theta_p} > N = \frac{\theta_A}{\theta_p} \gg Q = \frac{2\pi}{\theta_A}$$

(b)

FIGURE 28. Radial Line Spectrum

where N is a large number, or

$$\theta_p \ll \theta_A \quad (2b)$$

typically

$$W \ll \Delta R \quad (2c)$$

and

$$\Delta R \sim R_c \quad (2d)$$

However, for the moment, we will assume that both W and ΔR are very small so that both sinc functions in (1) are nearly unity and can be removed from the summation. The expression we are initially interested in is (see Fig 29)

$$I(\rho, \phi) = \sum_n e^{-iM \sin(\phi + n\theta_p)} \quad (3a)$$

where

$$M = 2\pi R_c \rho \quad (3b)$$

That is, we are considering the summations of the phase terms from a series of point sources at a radius R_c separated by the angle

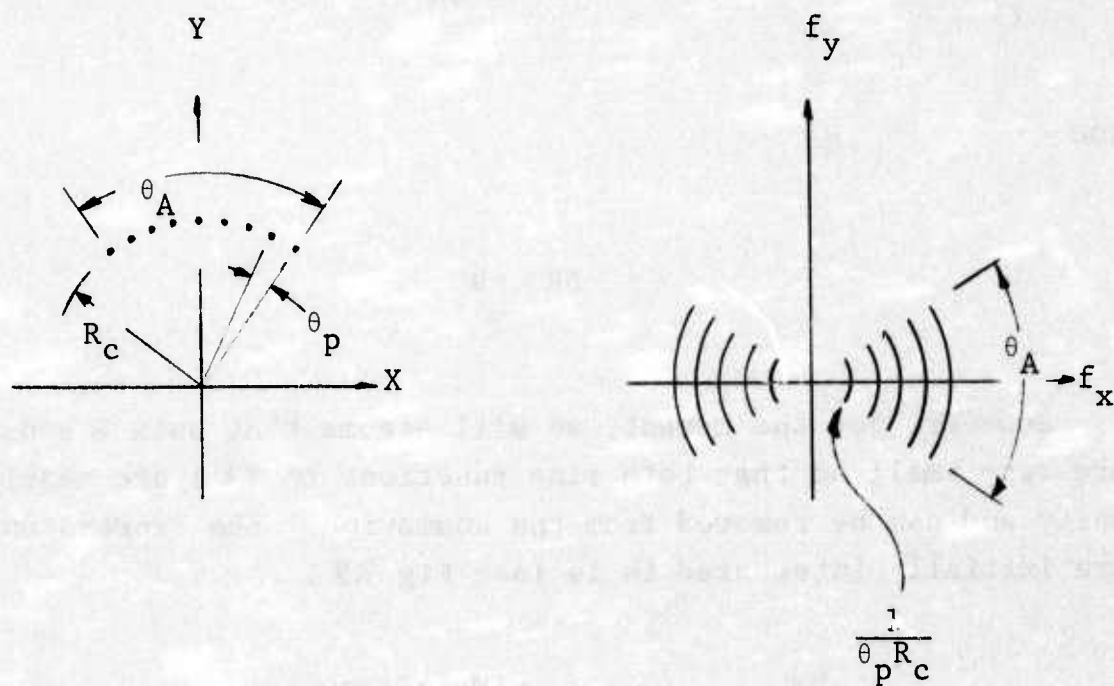


FIGURE 29. Circular Point Set Spectrum

θ_p . We then have

$$\begin{aligned}
 I(\rho, \phi) &= \sum_n \sum_{k=-\infty}^{\infty} J_k(M) e^{-ik(\phi + n\theta_p)} \\
 &= \sum_k J_k(M) e^{-ik\phi} \sum_n e^{-ikn\theta_p} \\
 &= \sum_k J_k(M) e^{-ik\phi} N \operatorname{sinc}_N\left(\frac{k\theta_p}{2\pi}\right)
 \end{aligned} \tag{4}$$

where we have defined

$$\operatorname{sinc}_N(t) \triangleq \frac{\sin(\pi Nt)}{N \sin(\pi t)} = \frac{1}{N} \sum_{n=-\frac{N-1}{2}}^{\frac{N-1}{2}} e^{+2\pi i n t} \tag{5a}$$

which has the characteristics:

$$\begin{aligned}
 \operatorname{sinc}_N(t) &= \sum_{n=-\infty}^{\infty} \operatorname{sinc}[N(t-n)] \\
 &= \operatorname{sinc}(Nt) * \pi(t)
 \end{aligned} \tag{5b}$$

$$\lim_{N \rightarrow \infty} N \operatorname{sinc}_N(t) = \pi(t) \tag{5c}$$

$$\operatorname{sinc}_N(n) = \begin{cases} (-1)^n & \text{if } N \text{ even} \\ 1 & \text{if } N \text{ odd} \end{cases} \tag{5d}$$

$$\text{sinc}_N\left(\frac{n}{N}\right) = 0 \quad \text{for } n \neq \text{integer times } N \quad (5e)$$

$$\text{sinc}_N(t) \leftrightarrow \sum_{n=-\frac{N-1}{2}}^{\frac{N-1}{2}} \delta(f-n) \quad (N \text{ odd}) \quad (5f)$$

$$\begin{aligned} \text{The full width of } \text{sinc}_N t \text{ about its main maxima} \\ \text{(to the first zero) is } = \frac{2}{N} \end{aligned} \quad (5g)$$

$$\text{All secondary sidelobes are less than } \frac{1}{N} \quad (5h)$$

and where

$$\pi(t) = \sum_{n=-\infty}^{\infty} \delta(t-n) \quad (5i)$$

We now let $\theta_p = \frac{2\pi}{P}$ where P is a (large) positive and odd integer. Then (4) becomes

$$I(\rho, \phi) = N \sum_k \text{sinc}_N\left(\frac{k}{P}\right) J_k(M) e^{-ik\phi} \quad (6)$$

Thus the main maxima occur when (see eq. (5d))

$$k = mP \quad m \text{ an integer} \quad (7)$$

which defines the m^{th} diffracted order. That is, only a few terms around

$$J_{mP}(M)e^{-imP} \quad (8)$$

are not significantly suppressed. The peak value for this term is found from considering the following characteristics for k large:

$$\max J_k(M) \approx .7k^{-1/3} \quad (9a)$$

$$\text{when } M \approx k \quad k \gg 1 \quad (9b)$$

$$\begin{aligned} \text{half width of this main peak} &\approx k^{1/3} \\ \text{area under main peak} &\approx 1.4 \end{aligned} \quad (9c)$$

Thus, taking $mP = M$ to satisfy condition (9a) we have from eqs. (2a) and (3b) that the Bessel function of order mP peaks at ρ_m and has a half width $\Delta\rho_m$ where

$$\rho_m = \frac{m}{\theta_p R_c} \quad (10)$$

and

$$\Delta \rho_m = \frac{\rho_m}{(mP)^{2/3}} \quad (11)$$

ρ_m is m times the tangential frequency of the point sources and $\Delta \rho_m$ is a small portion of ρ_m since P is a large number.

Let us now find the extent of the m^{th} order. Recall from (2a) that $N < P$. We let $P/N = Q$ where we assume that Q is an odd integer. Note that $\theta_A = 2\pi/Q$. Hence, as indicated in Figure 30, there are Q terms contained within the half-width of the main maxima of the sinc_N function. Thus for the m^{th} order the signal is

$$\begin{aligned} I_m(\rho, \phi) &\approx \sum_{k = mP - \frac{Q-1}{2}}^{mP + \frac{Q-1}{2}} .7(mP)^{-1/3} e^{ik\phi} \\ &= .7(mP)^{-1/3} Q e^{imP\phi} \text{sinc}_Q \frac{\phi}{2\pi} \end{aligned} \quad (12)$$

Since $Q = \frac{2\pi}{\theta_A}$ then the sinc_Q function limits the m^{th} order energy to within the angles $\phi = \pm \frac{\theta_A}{2}$. Note that due to the periodicity of 2π for the sinc_Q function that all its primary maxima fall on top of each other. From general symmetric considerations for FT's we know that a symmetrically placed order to m must exist. It comes from placing the negative value of m in eq (7). From eq (12) we also see that the orders slowly die in intensity by $m^{-2/3}$.

The range of ρ can be found from the ranges of indices allowed by sinc_N since the Bessel functions main peak width greatly exceeds that of sinc_N (see eq. 9). The index range is from $(mP - \frac{Q-1}{2})$ to $(mP + \frac{Q-1}{2})$, or

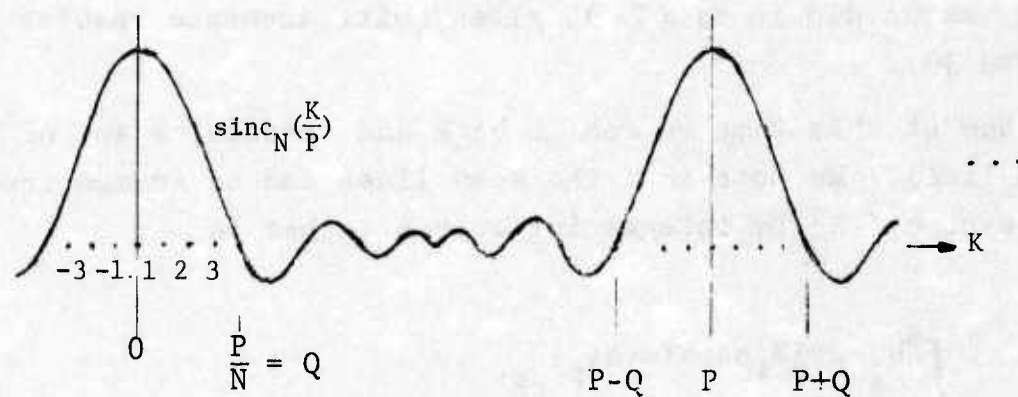


FIGURE 30. The Function $\text{Sinc}_N(\frac{k}{p})$

$$\frac{mP - \frac{Q-1}{2}}{2\pi R_c} \leq \rho \leq \frac{mP - \frac{Q-1}{2}}{2\pi R_c}$$

or

$$\frac{m}{R_c \theta_p} - \frac{1}{2\theta \frac{R_c}{A}} \leq \rho \leq \frac{m}{R_c \theta_p} + \frac{1}{2\theta \frac{R_c}{A}} \quad (13)$$

Thus ρ is limited to the small range of $\frac{\rho_1}{N}$ about the order center which implies that substituting the peak value for the Bessel function, as we did in eq (12), gives quite accurate results (see Figure 30).

Now at this time we can go back and consider a set of N narrow scan lines. We note that the scan lines can be formed from the expression (3) by integrating over R_c , that is

$$\begin{aligned} & \int_{R_a}^{R_b} e^{-2\pi i R'_c \rho \sin(\phi + n\theta_p)} dR'_c \\ &= \Delta R e^{-2\pi i R_c \rho \sin(\phi + n\theta_p)} \text{sinc}[\Delta R \rho \sin(\phi + n\theta_p)] \end{aligned} \quad (14)$$

However, rather than integrate immediately the expression (14) we will delay the integration until after the summation. That is, we take expression (12) to be approximated by

$$C(\phi) \delta\left(\rho - \frac{m}{\theta \frac{R_c}{A}}\right)$$

where

$$C(\phi) = 1.4(2\pi)^{-1/3} Q e^{im\phi} \text{sinc}_Q\left(\frac{\phi}{2\pi}\right)$$

Then

$$\begin{aligned} \frac{I_m}{C(\phi)} &\approx \int_{R_c - \frac{\Delta R}{2}}^{R_c + \frac{\Delta R}{2}} \delta\left(\rho - \frac{m}{p} r\right) dr \\ &= \int_{-\infty}^{\infty} \text{rect}\left(\frac{r - R_c}{\Delta R}\right) \frac{\delta\left(r - \frac{m}{p} \rho\right)}{\rho^2} dr \\ &= \frac{1}{\rho^2} \text{rect}\left[\frac{\rho - \rho_m}{\frac{\Delta R}{R_c} \rho}\right] \\ &= \frac{1}{\rho^2} \text{rect}\left[\frac{\rho - \hat{\rho}_m}{\frac{\Delta R}{R_c} \hat{\rho}_m}\right] \end{aligned} \quad (15)$$

where

$$\hat{\rho}_m = \frac{\rho_m}{1 - \left(\frac{\Delta R}{2R_c}\right)^2}$$

That is, the m^{th} order is centered at $\hat{\rho}_m$ and has a width $\frac{\Delta R}{R_c} \hat{\rho}_m$.

If $\Delta R \ll R_c$ then ρ_m can be substituted for $\hat{\rho}_m$.

Thus, the effect of the sinc term in (14) is to disperse the spectrum orders proportional to the order number. Hence the orders will tend to overlap at high order numbers. We would expect the first sinc term in (1) to also disperse the signal, but since W is small its effect is not expected to be significant, except to reduce the intensity of the higher orders.

We would now like to go back to eq. (3c) and allow a sinusoidal modulation of the point sources such that

$$\begin{aligned} I(\rho, \phi) &= \sum_n^N \cos(\epsilon n) e^{-iM \sin(\phi + n\theta_p)} \\ &= \frac{N}{2} \sum_k J_k(M) \left[\text{sinc}_N\left(\frac{k}{P} + \frac{\epsilon}{2\pi}\right) + \text{sinc}_N\left(\frac{k}{P} - \frac{\epsilon}{2\pi}\right) \right] e^{-ik\phi} \end{aligned}$$

Thus, using the same techniques as before we find that the m^{th} order is now split and given by

$$\rho_{m\pm} = \frac{1}{\theta_m R_c} \left(m \pm \frac{\epsilon}{2\pi} \right)$$

We note that the order will move by one whole order position for $\epsilon = \pm 2\pi$.

Modulated Scan Lines

Let us now consider a sinusoidal amplitude modulation of the scan lines of the form $1 + A \cos(2\pi F r + n\epsilon)$ where F is the spatial frequency and ϵ is the synchronization factor. It is straightforward to see that eq. (1) is now replaced by an equation that is

identical except that the second sinc term is replaced by

$$\begin{aligned} & \text{sinc} [\Delta R \rho \sin(\phi + n\theta_p)] \\ & + \frac{A}{2} \left\{ \text{sinc} [\Delta R \rho \sin(\phi + n\theta_p) - \Delta R F] e^{in\epsilon + 2\pi i R_c F} \right. \\ & \left. + \text{sinc} [\Delta R \rho \sin(\phi + n\theta_p)] + \Delta R F e^{-in\epsilon - 2\pi i R_c F} \right\} \end{aligned} \quad (16)$$

This form of the equation is convenient for computer analysis but not for analytical understanding. Rather, we start with eq. (4), but where the $J_k(M)$ term is replaced by

$$\begin{aligned} E &= \int_{R_a}^{R_b} \cos(2\pi Fr + n\epsilon) J_k(2\pi \rho r) dr \\ &= \frac{1}{2} \int_{-\infty}^{\infty} \text{rect} \frac{r - R_c}{\Delta R} J_k(2\pi \rho r) e^{2\pi i r F} dr e^{in\epsilon} + \text{c.c.} \\ &= \frac{1}{2} \left[\Delta R \text{sinc}(\Delta R F) e^{-2\pi i F R_c} \right] *_F A_k(F, \rho) e^{in\epsilon} + \text{c.c.} \end{aligned} \quad (17)$$

where $*_F$ represents convolution with respect to F and $A_k(F, \rho)$ is the FT of the Bessel function, i.e.

$$\begin{aligned} A_k(F, \rho) &= \int_{-\infty}^{\infty} J_k(2\pi \rho r) e^{-2\pi i r F} dr \\ &= \frac{(-i)^k T_k\left(\frac{F}{\rho}\right) \text{rect}\left(\frac{F}{2\rho}\right)}{\pi \sqrt{\rho^2 - F^2}} \end{aligned} \quad (18)$$

Here $T_k(\cdot)$ is the k^{th} order Chebyshev polynomial which has the following properties of interest

$$T_k(\cos\alpha) = \cos(k\alpha)$$

$$T_k(-x) = (-1)^k T_k(x) \quad (19)$$

$$T_0(x) = 1$$

For the moment, we will assume that ΔR approaches infinity. That is, we substitute

$$\delta(F) = \lim_{\Delta R \rightarrow \infty} \Delta R \text{sinc}(\Delta R F) \quad (20)$$

for the sinc function in (17). Notice that this implies that the scan lines pass through the origin and extend to $\pm\infty$. We can then write for (17)

$$E = A_0(F, \rho) \cos(k\alpha) \cos(n\epsilon + \frac{\pi}{2}k) \quad (21)$$

where we have let

$$\cos\alpha = \frac{F}{\rho} \quad (22)$$

which can be done since in eq. (18) the rect function implies $|\rho| \geq F$ (assumed F is positive). We note from (18) that

$$A_0(F, \rho) = \frac{\text{rect}(F/2\rho)}{\pi\sqrt{\rho^2 - F^2}} \leftrightarrow J_0(2\pi\rho r) \quad (23)$$

Eq. (6) now becomes

$$I'(\rho, \phi) = NA_0(F, \rho) \sum_k^\infty \sum_n^N \quad (24)$$

$$\cdot \cos(k\alpha) \cos(n\epsilon + \frac{\pi}{2}k) e^{-ik(\phi + n\theta_p)}$$

where it is understood that all summations are symmetric, i.e.

$$\sum_n^N \triangleq \sum_{n=-\frac{N-1}{2}}^{\frac{N-1}{2}}, \quad \sum_n^\infty \triangleq \sum_{n=-\infty}^\infty \quad (25)$$

We now use the identity (see Figure 31)

$$\begin{aligned} & \sum_k^\infty \sum_n^N e^{-2\pi i k(A+nB)} \\ &= \sum_k^\infty e^{-2\pi i kA} \text{sinc}_N(kB) \\ &= \sum_k^\infty \sum_n^N \delta(A+nB-k) \end{aligned} \quad (26)$$

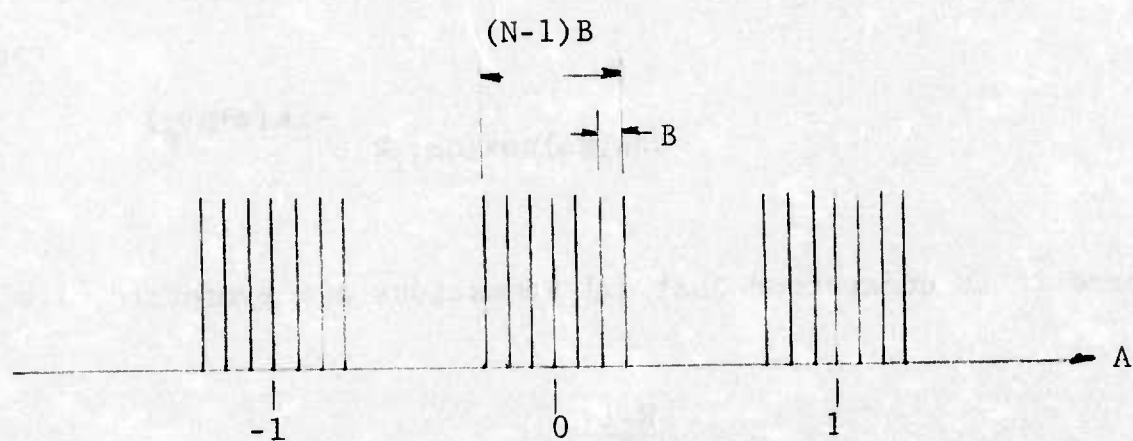


FIGURE 31. The Function $\left[\text{III}\left(\frac{A}{B}\right) \text{rect}\left(\frac{A}{NB}\right) \right]_A^* \text{III}(A)$

$$= \pi \left(\frac{A}{B} \right) \text{rect} \left(\frac{A}{NB} \right) *_{\frac{A}{A}} \pi(A)$$

to write (24) as

$$I'(\rho, \phi) = \frac{QN}{4} A_O(F, \rho) \left\{ \left[\pi \left(\frac{\phi}{\theta_p} \right) \text{rect} \left(\frac{\phi}{\theta_A} \right) e^{i \left(\frac{\epsilon \phi}{\theta_p} \right)} \right] *_{\phi} \left[\delta \left(\phi + \alpha + \frac{\pi}{2} \right) + \delta \left(\phi + \alpha - \frac{\pi}{2} \right) + \delta \left(\phi - \alpha - \frac{\pi}{2} \right) \right] \right\} \quad (27)$$

In order to consider the physical meaning of this expression we first note that the delta functions represent a locus given by

$$\phi \pm \alpha \pm \frac{\pi}{2} = 0 \quad (28)$$

which gives

$$\sin \phi = \pm \cos \alpha \quad (29)$$

or

$$f_y = \pm F \quad (30)$$

since $\rho \sin \phi = f_y$ and $\rho \cos \alpha = F$. That is, these are straight lines with y-axis intercept $\pm F$. When convolved with the rect function

(with respect to the angle ϕ) we see that it restricts ϕ to angle θ_A about the directions $(\pm\alpha \pm \frac{\pi}{2})$, which of course varies with ρ . For $\rho = F$, that is, on the circle of radius F , we have that $\alpha = 0$ and hence ϕ is confined to θ_A about $\pm \frac{\pi}{2}$. The π function represents a high frequency fringe system whose loci are given by

$$\phi \pm \alpha \pm \frac{\pi}{2} = m\theta_p \quad m = 0, \pm 1, \dots \quad (31)$$

or

$$F = \cos(m\theta_p)f_x \pm \sin(m\theta_p)f_y \quad (32)$$

This represents straight lines tangent to a circle of radius F and with slope $m\theta_p$. Similarly the loci of constant phase as represented by the exponent term are straight lines tangent to the same circle but with slope $m\theta_p/\epsilon$. The term $A_o(F, \rho)$ limits the energy to outside the circle $\rho = F$ and gives a signal die off proportional to $(\rho^2 - F^2)^{-1/2}$.

The above results have a straightforward physical interpretation. A single sinusoidal modulated scan line of infinite length has a FT that is composed of 3 parallel lines, one through the origin and the other two displaced by $\pm F$ from the origin such that they are tangent to the circle $\rho = F$. Figures 32a to 32c show various relationships between the parameters of the transform lines (T-lines). We note that for any circle with radius $\rho \geq F$ the T-lines cut the circumference over a range of θ_A into equal increments of arc length $\rho\theta_p$. This, of course, also holds true for $F = 0$, which represents no modulation on the scan lines. If we now consider the implications of eq. (10) for this latter case we see that the m^{th} order

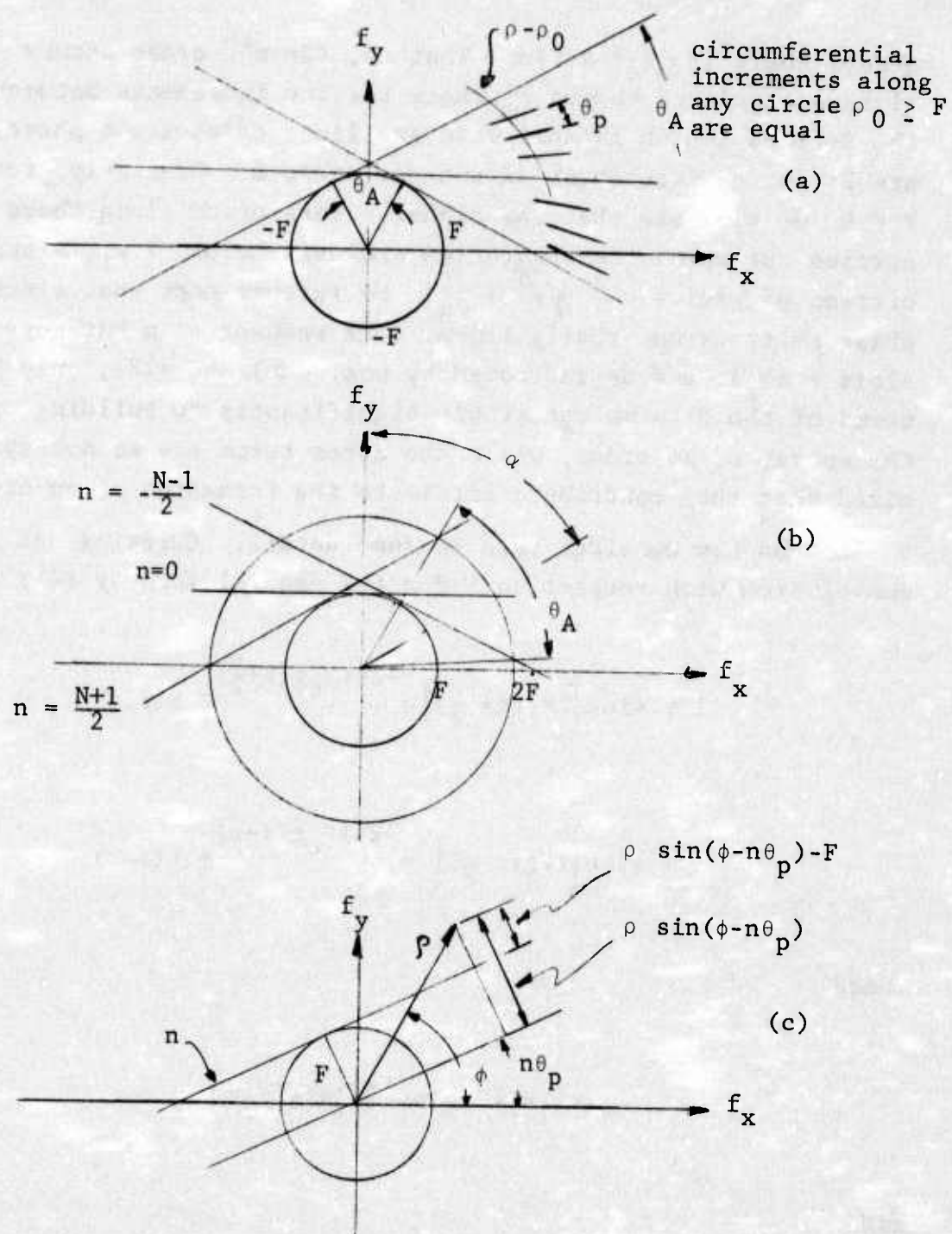


FIGURE 32. Frequency Plane Structure

occurs where $2\pi\rho_p R_c \rho = 2\pi m$. That is, the m^{th} order occurs along a circle of radius ρ_m where the arc increments between the T-lines (which in this case are lines of constant phase) are 2π phase differences of integer order m . Similarly, for $F \neq 0$, we will see that the higher orders occur along those circles for which the separation criteria holds, i.e., along circles of radius $\rho = \sqrt{F^2 + \rho_m^2}$. We further note that since the phase shift is not really linear with respect to n but goes as $\sin(\phi + n\theta_p)$, and as indicated by eqs. (6) and (12), only Q terms of the N terms contribute significantly to building up the energy of an order, while the other terms are so non-synchronized that they contribute little to the formation of an order.

Let us now consider this in some detail. Carrying out the convolution with respect to F for the general form of (27) gives

$$I = \text{sinc}\left[\Delta R g\left(\phi + \frac{\pi}{2}\right)\right] e^{-2\pi i R_c g\left(\phi + \frac{\pi}{2}\right)} \underset{\phi}{*} B(\phi, \epsilon) \\ + \text{sinc}\left[\Delta R g\left(\phi - \frac{\pi}{2}\right)\right] e^{-2\pi i R_c g\left(\phi - \frac{\pi}{2}\right)} \underset{\phi}{*} B(\phi, \epsilon) \quad (33)$$

where

$$g(\phi) = -2\pi \sin\left(\frac{\phi - \alpha}{2}\right) \sin\left(\frac{\phi + \alpha}{2}\right) \quad (34)$$

and

$$B(\phi, \epsilon) = \sum_n^N e^{in\epsilon} \delta(\phi - n\theta_p) \\ = \pi \left(\frac{\phi}{\theta_p}\right) \text{rect}\left(\frac{\phi}{\theta_A}\right) e^{i\left(\frac{\epsilon\phi}{\theta_p}\right)} \quad (35)$$

Obviously the maxima for the sinc functions occur when condition (28) is satisfied, that is, these maxima occur along the lines $f_y = \pm F$. With $R_c \rho > \Delta R \rho \gg 1$ and $\alpha \gg 0$ the four maxima are physically separated (this does not occur in the zero order, which we will later consider in detail). Considering only the maximum for which $\phi \approx \pi/2 - \alpha$ we can make the approximation

$$g(\phi - \frac{\pi}{2}) \approx -2\rho \sin \alpha \sin(\phi'/2) \quad (36)$$

where

$$\phi' = \phi + \alpha - \pi/2 \quad (37)$$

The term of interest then becomes

$$\sum_n^N \text{sinc} \left[2\rho \Delta R \sin \alpha \sin \left(\frac{\phi' - n\theta}{2} \right) \right] \exp \left[4\pi i R_c \rho \sin \alpha \sin \left(\frac{\phi' - n\theta}{2} \right) + n\epsilon \right] \quad (38)$$

Comparison of (38) for $\epsilon = 0$ with the original expression (1) shows that it has exactly the same form. Thus the same type of analysis as for the original section will hold if we substitute

$$\rho \rightarrow \rho \sin \alpha = \sqrt{\rho^2 - F^2}$$

$$\phi \rightarrow \phi' = \phi - \alpha - \pi/2$$

Then the m^{th} order radius (for $\Delta R \rightarrow 0$) is given by

$$\rho_m' = \sqrt{F^2 - \left(\frac{m - \epsilon/2\pi}{\theta_p R_c} \right)^2}$$

and for $\Delta p \ll R_c$ the order has a width of $\Delta R_{\rho_m}/R_c$ along the variable $\rho \sin \alpha$. The angle ϕ' is confined to $\pm \theta_A/2$. These effects are illustrated in Figure 24.

The zero-order has to be considered in detail by itself since it need not satisfy some of the assumed approximations. In fact, its character is quite different than that of the higher orders. The energy to form the higher orders comes from the diffraction of the grating formed by the scan lines, whereas, the zero-order does not use this diffraction effect but rather the diffraction from the radial modulation. Consider that the tangential direction along the circle $\rho = F$ (i.e., the first order position) is a direction orthogonal to the phase variation direction (see Figure 32), and hence the phases can not add up as for the higher orders. This can be seen mathematically in that the higher orders are due to the primary maxima of the Bessel function, whereas, the zero-order is a resonance condition with the asymptotic oscillation of the Bessel function. That is, we substitute the asymptotic approximation

$$J_k(2\pi \rho r) = \frac{1}{\pi \sqrt{\rho r}} \cos(2\pi \rho r - \frac{\pi k}{2} - \frac{\pi}{4})$$

into this general form of eq. (17) to get

$$I = \frac{1}{\pi \sqrt{\rho R_c}} \sum_n^N \sum_k^\infty e^{ik(\phi + n\theta_p)} \int_{R_a}^{R_b} dr \cos(2\pi Fr + n\epsilon) \cos(2\pi \rho r - \frac{\pi k}{2} - \frac{\pi}{4})$$

where we have let $1/\sqrt{r} = 1/\sqrt{R_c}$ since $1/\sqrt{r}$ does not change significantly over the range $R_a < r < R_b$. Then we find that

$$I = \frac{N\Delta R}{2\pi\sqrt{\rho R_c}} \text{sinc } \Delta R(F_r - \rho)$$

$$\cdot \left[\text{rect} \left(\frac{\phi}{\theta_A} \right) \pi \left(\frac{\phi}{\theta_p} \right) e^{i \left(\frac{\phi}{\theta_p} \right)} e^{2\pi i (F-\rho) R_c} c_{\phi}^* \delta \left(\phi + \frac{\pi}{2} \right) \right.$$

$$\left. + \text{c.c. } c_{\phi}^* \delta \left(\phi - \frac{\pi}{2} \right) \right]$$

Thus the zero order is confined to $\pm \frac{\theta_A}{2}$ about $\phi = \pm \frac{\pi}{2}$ and has a radial width of about $\frac{1}{\Delta R}$ about $\rho = F$. We note that the peak intensity at $\rho = F$ decreases as $1/F$ (while the arc length of the order increases proportional to F keeping the total energy in the order constant).

Thus, this completes the construction of Figure 24, which explains the experimental results given in Section 6.3.

6.6 OPTICAL RECTIFICATION

Analysis of the spatial frequency spectrum which results when data is recorded in a polar rather than rectangular format indicates that the frequency plane distribution may not be suitable for a spectrum analyzer application without some modification in the processing optics. Recall from Sections 6.3 and 6.4 that a single frequency recorded in the polar format results in a Fourier frequency plane distribution that is spread over an arc rather than the point-like spot obtained with the rectangular input data format. It appears that frequency resolution for un-synchronized sinusoidal data (Section 6.3) may be compromised because of the arc distribution.

Several approaches to a correction for the polar format may be possible. One approach considered during this program was to provide, as part of the data processing optics, optical elements which convert the polar data into rectangular data (optical rectification). It must be noted, however, that since coherent optical processing of phase data is being considered, the light field amplitude and phase rather than its intensity must be properly preserved. This is in contrast to some extent to the design of an optical rectification scheme for image projection devices.

The use of a spherical lens tilted relative to the recorded data plane allows the convergent scan lines of a polar recording to become parallel. However, this causes the ends of the scan lines to line-up on a curve rather than a straight line as with a rectangular raster and some loss in resolution also occurs. Added provisions for straightening the raster edge and correcting for resolution loss were considered but the methods pursued during the limited effort expended on this task did not result in a satisfactory solution.

7
CONCLUSIONS AND RECOMMENDATIONS

Evaluation of the performance properties of the experimental model real-time thermoplastic modulator for use with a coherent optical processing channel was accomplished. Recording bandwidths to 70 MHz; spatial bandwidth of 30 c/mm; dynamic range of 40 db; and, high optical quality recording apertures over several square inches were realized. Optical processing for the spectrum analyzer application with either rectangular or polar input data recording formats was analyzed and the unusual properties associated with polar data were clearly established. Fabrication and coating methods for a large 15" diameter rotatable recording disc and 5" recording plate were refined to give thermoplastic recording surface of high thickness uniformity.

This program has served to establish the feasibility of employing a thermoplastic modulator as the means for high quality and high density data insertion into a coherent optical processing channel on a real-time basis, thus allowing a more practical approach to utilization of the excellent properties of coherent optical processing.

It is recommended that the technology base established in this program be extended in the areas of (1) further design refinement for increased spatial bandwidth (≈ 100 c/mm) and examination of material properties; (2) study of system signal response for increased dynamic range (≈ 60 db); and (3) evaluation of additional real-time optical computer application areas such as SAR data processing, pattern recognition, hybrid optical-digital systems and special purpose display devices. The thermoplastic modulator should also be considered as a device usable for construction of computer generated holographic optical elements or other types of thin film optical components.

REFERENCES

1. Real-Time Modulator for Coherent Optical Processing, Air Force Technical Report, AFAL-TR-73-88, May 1973, I. Cindrich, G. Currie, C. Leonard.
2. Coherent Optical Computers, K. Preston, Jr., McGraw-Hill Book Company, 1972.